
Class Distribution Shifts in Zero-Shot Learning: Learning Robust Representations

Yuli Slavutsky

Department of Statistics and Data Science
The Hebrew University of Jerusalem
Jerusalem, Israel
yuli.slavutsky@mail.huji.ac.il

Yuval Benjamini

Department of Statistics and Data Science
The Hebrew University of Jerusalem
Jerusalem, Israel
yuval.benjamini@mail.huji.ac.il

Abstract

Zero-shot learning methods typically assume that the new, unseen classes that are encountered at deployment, come from the same distribution as training classes. However, real-world scenarios often involve class distribution shifts (e.g., in age or gender for person identification), posing challenges for zero-shot classifiers that rely on learned representations from training classes. In this work, we propose a model that assumes that the attribute responsible for the shift is unknown in advance, and show that standard training may lead to non-robust representations. To mitigate this, we propose an algorithm for learning robust representations by (a) constructing synthetic data environments via hierarchical sampling and (b) applying environment balancing penalization, inspired by out-of-distribution problems. We show that our approach improves generalization on diverse class distributions in both simulations and real-world datasets.

1 Introduction

Zero-shot learning [14, 27] tackles classification in scenarios where, in deployment, the classifier encounters new classes that were unseen during training (*open-world* classification). Zero-shot systems are used in extreme multi-class applications such as face or voice recognition [19] to match multiple observations from the same person, and generally for learning data representations [2].

Class distribution shifts usually refer to changes in class prevalence between training and testing, assuming a fixed set of classes. However, in zero-shot learning, a key question arises: do the new classes follow the same distribution as the training classes? Most zero-shot methods rely on the assumption that the classes are indeed sampled from the same distribution. This assumption is implicitly incorporated into the design of test sets [57, 16], and is explicitly used to assess the ability of zero-shot classifiers to generalize [59, 48].

In practice, training classes are often chosen based on convenience and accessibility during the data collection. Even with careful collection, the distribution of classes may shift over time, leading to a different distribution. For instance, consider a face recognition system deployed in a building located in a neighborhood undergoing demographic changes.

Class distribution shifts pose significant challenges for zero-shot classifiers, since they rely on learning from the training classes to distinguish new, unseen ones. Typically, these classifiers are trained by minimizing the loss over the training set to achieve effective separation among the training classes. However, this approach may result in poor performance when confronted with distributions that significantly differ from the class distribution in the training data. Notably, in person re-identification, this concern gained attention from a fairness perspective with respect to gender bias [15, 23], age

bias [5, 33, 50] and racial bias [39, 54]. In all these examples it is known which variable (i.e., gender, age, race) is expected to cause the distribution shift.

However, in real-world scenarios, it is usually unknown during training which attribute will be responsible for a future distribution shift. In such cases, approaches based on collecting balanced datasets or re-weighting training examples [54, 41, 53] are inapplicable. Furthermore, while class distribution shifts have been extensively studied in the standard setting of supervised learning (see Appendix A), this previous work assumes a *closed-world* setting. It does not account for new classes at test time, and only addresses changes in the prevalence of fixed classes between training and testing. Consequently, class distribution shifts in zero-shot learning remain untreated.

As a first contribution of this work (§3), we study the effects of class distribution shifts on contrastive zero-shot learning, by proposing and analyzing a parametric model. We identify conditions where minimizing loss in this model leads to representations that perform poorly on shifted distributions.

We then use the insights gained from this model to present our second contribution (§4): a first algorithm for learning robust representations against class distribution shifts in zero-shot classifiers. Our proposed approach constructs *artificial data environments* with diverse attribute distributions using hierarchical sub-sampling, and applies an *environment balancing* criterion inspired by out-of-distribution (OOD) methods. We assess the effectiveness of our method through both simulations and experiments on real-world datasets, demonstrating its enhanced robustness in §5.

1.1 Problem Setup

Let $\{z_i, c_i\}_{i=1}^{N_z}$ be a labeled set of training data points $z \in \mathcal{Z}$ and classes $c \in \mathcal{C}$, such that c_i is the class of z_i . In this work we focus on verification algorithms that in order to allow for the *open-world* classification, determine whether a pair of data-points $x_{ij} := (z_i, z_j)$ belong to the same class. For instance, in person re-identification the task is to identify whether two data points (e.g., face images or voice recordings) belong to the same person. We denote this by y_{ij} , where $y_{ij} = 1$ if $c_i = c_j$ and $y_{ij} = 0$ otherwise. When the identity of each data point in the pair is not important, we use a single index for simplicity, namely (x_k, y_k) .

We assume that each class c is characterized by some attribute A . We assume that the training classes are sampled from $P_C(c)$, the test classes are sampled according to $Q_C(c)$, and that the two distributions differ solely due to a shift in the attribute A :

$$P_C(c) = \int P_{C|A}(c|a) \mathbf{P}_A(a) da, \quad Q_C(c) = \int P_{C|A}(c|a) \mathbf{Q}_A(a) da. \quad (1)$$

We assume that the variable A is unknown, and that both in training and in testing, data points $z \in \mathcal{Z}$ for each class are sampled according to $P_{Z|C}(z|c)$. For instance, revisit the person identification example where each person is a class. If the attribute A is binary (e.g., a_1 is blond and a_2 is dark-haired), then $P(C|A = a_1)$ represents the distribution of blond individuals, and $P(C|A = a_2)$ over dark haired ones. The training classes might be predominantly sampled from the blond population $P(A = a_1) = \rho_{\text{tr}} = 0.8$, while test classes from $Q(A = a_1) = \rho_{\text{tr}} = 0.1$.

We focus on verification techniques that are based on *deep metric learning* methods (for reviews see [43, 34]) such as contrastive-learning [17], Siamese neural networks [24], triplet networks [20], and more recent variations [35, 49, 56, 58]. These methods learn a representation function that maps data-points to a representation space $g : \mathcal{Z} \rightarrow \hat{\mathcal{Z}}$, so that examples from the same class are close (in a predefined distance function $d(\cdot, \cdot)$), whereas those from different classes are farther apart.

We assume that g is a neural network that is trained by optimizing a deep-metric-learning loss, such as the contrastive loss [17]:

$$\ell(z_i, z_j, y_{ij}; d_g) := y_{ij} d_g^2(z_i, z_j) + (1 - y_{ij}) \max\{0, m - d_g(z_i, z_j)\}^2 \quad (2)$$

where $m \geq 0$ is a predefined margin. In our theoretical results, we analyze the no-Hinge contrastive loss (see Appendix B for additional details):

$$\tilde{\ell}(z_i, z_j, y_{ij}; d_g) := y_{ij} d_g^2(z_i, z_j) + (1 - y_{ij}) (m - d_g(z_i, z_j))^2. \quad (3)$$

To assess the quality of the representation we treat distances between representations $d_g(z_i, z_j) := d(g(z_i), g(z_j))$ as classification scores. Following common practice in the field (see, for example,

[47, 22]), we use the area under the receiver operating characteristic curve (AUC) to evaluate the representation, allowing for threshold-agnostic assessment:

$$AUC(g) := P(d_g(z_i, z_j) < d_g(z_u, z_v) | y_{ij} = 1, y_{uv} = 0). \quad (4)$$

Our goal is to learn a representation g that is robust to class attribute shifts. That is, such that for an unknown shifted distribution Q_A , the performance $\mathbb{E}_{Q_A} [AUC(g)]$ does not significantly deteriorate compared to the performance obtained on the training distribution P_A .

2 Background on Environment Balancing Methods in OOD Generalization

The field of OOD generalization gained attention since the work of Peters et al. [36], [37]. It deals with closed-world classification where training data is gathered from multiple environments E_{train} . In this setting it is assumed that in each environment $e \in E_{\text{train}}$, examples share the same joint distribution $P_{C,Z}^e(c, z)$, but across environments e , the joint distribution changes, often due to variations in $P_{Z|C}^e(z|c)$. A prominent example [1] involves classifying images of cows and camels and demonstrates how an algorithm relying on background cues during training (e.g., cows in green pastures, camels in deserts) performs poorly on new images of cows in sandy backgrounds.

Several approaches that rely on access to diverse training environments were proposed to identify stable relations between the data point z and its class c . Examples of such stable relations include choosing causal variables using statistical tests [42], leveraging conditional independence induced by the common causal mechanism [9], and using multi-environment calibration as a surrogate for OOD performance [52].

Most relevant to our work are methods that aim to balance the loss over multiple environments. Consider a representation $g = g_\theta$ that is a neural network parameterized by θ , trained to optimize an objective of the form

$$\min_{\theta} \sum_{e \in E_{\text{train}}} \ell^e(g_\theta) + \lambda R(g_\theta, E_{\text{train}}) \quad (5)$$

where $\ell^e(g_\theta)$ is the empirical loss obtained on the environment e , E_{train} is the set of all training environments, R is a regularization term designed to balance performance over multiple environments, and λ is a regularization factor weighing between the Empirical Risk Minimization (ERM) term and the balance penalty. We present below three such methods, which we later refer to.

Invariant Risk Minimization (IRM) [1] aims to find data representations g_θ such that the optimal classifier w on top of that data representation $w \circ g_\theta$, is shared for all environments. The authors therefore propose minimizing the sum of environment losses $\ell^e(w \circ g_\theta)$ over all training environments, such that $w \in \arg \min_{w'} \ell^e(w' \circ g_\theta) \quad \forall e \in E_{\text{train}}$. However, since it is too hard to optimize, a relaxed objective is proposed instead. It takes the form of Equation 5 with a regularization that measures how close w is to minimizing $\ell^e(w \circ g_\theta)$: $R_{\text{IRMv1}}^e(g_\theta) = \|\nabla_{w|w=1} \ell^e(w \cdot g_\theta)\|^2$.

Note that for loss functions, for which optimal classifiers can be written as conditional expectations, the original IRM objective is equivalent to the requirement that for all environments $e, e' \in E_{\text{train}}$, $\mathbb{E}_{P_{C,Z}^e} [c|g(z) = h] = \mathbb{E}_{P_{C,Z}^{e'}} [c|g(z) = h]$, where $P_{C,Z}^e$ and $P_{C,Z}^{e'}$ are the joint data distribution in the respective environments.

Calibration Loss Over Environments (CLOvE) [52] leverages the equivalence above to establish a link between multi-environment calibration and invariance for binary predictors ($c \in \{0, 1\}$). The proposed regularizer is based on *Maximum Mean Calibration Error* (MMCE) [26]. Let $s : \hat{\mathcal{Z}} \rightarrow [0, 1]$ be a classification score function applied on the representation $s \circ g$, and $s_i = \max\{s \circ g(z_i), 1 - s \circ g(z_i)\}$ be the *confidence* on the i -th data point. Denote by $b_i = \mathbb{I}\{|c_i - s_i| < \frac{1}{2}\}$ the *correctness*, and let $K : \mathbb{R} \times \mathbb{R} \rightarrow \mathbb{R}$ be a universal kernel. Let Z^e denote the training data in the environment e . The authors propose using MMCE as a regularization in an objective formed as Equation 5 with $R_{\text{MMCE}}^e(s, g_\theta) = \frac{1}{m^2} \sum_{z_i, z_j \in Z^e} (b_i - s_i)(b_j - s_j) K(s_i, s_j)$.

Variance Risk Extrapolation (VarREx) proposed by Krueger et al. [25], is based on the observation that reducing differences in loss (risk) across training domains can reduce a model's sensitivity to a wide range of distribution shifts. The authors found that using the variance of losses as a regularizer

is stabler and more effective compared to other penalties. Therefore, they propose the following regularization term for n training environments: $R_{\text{VarREx}}(g_\theta, E_{\text{train}}) = \text{Var}(\ell^{e_1}(g_\theta), \dots, \ell^{e_n}(g_\theta))$.

While simple and intuitive, this approach assumes that losses on different environments accurately reflect the classifier’s performance. However, as discussed in §4, this is often not the case for deep metric learning losses.

3 Parametric model of class distribution shifts in zero-shot learning

In this section, we introduce a parametric model of class distribution shifts. This model shows that in zero-shot learning, even if the conditional distribution of data given the class $P(z|c)$ remains the same between training and testing, a shift in the class distribution from $P(c)$ to $Q(c)$ can cause poor performance on newly encountered classes, sampled from the shifted distribution $Q(c)$.

Assume that for all classes the data points $z_i \in \mathbb{R}^d$ are sampled from $z_i|c_i \sim \mathcal{N}(c_i, \Sigma_z)$, where $\Sigma_z = \nu_z \cdot I_d$ and I_d is the identity matrix. Let the attribute A indicate the type to which a class c belongs, and assume there are two types: a_1 and a_2 , such that in training a_1 is the majority type with $P(a_1) = 1 - \rho_{\text{tr}} \gg 0.5$, while at test time a_2 is the majority type with $Q(a_1) = 1 - \rho_{\text{te}} \ll 0.5$.

Assume that the classes c_i are drawn according to $c_i \sim \mathcal{N}(0, \Sigma_a)$ for $a \in \{a_1, a_2\}$. We construct the model such that differences between the training class distribution $P(c)$ and the test distribution $Q(c)$ arise solely from a shift in the mixing probabilities of an unknown attribute A (see Equation 1). Therefore, we define Σ_a as a diagonal matrix with replicates of three distinct values on its diagonal: ν_0, ν^+, ν^- . Let $0 < \nu^- < \nu_z \leq \nu_0 < \nu^+$. Then, in the coordinates corresponding to ν_0 and ν^+ data points from different classes are well separated, whereas in the coordinates corresponding to ν^- they are not. Assume the coordinates corresponding to ν_0 are shared for both types, but ν^+ and ν^- are swapped:

$$\begin{aligned}\Sigma_{a_1} &= \text{diag}(\overbrace{\nu_0, \dots, \nu_0}^{d_0}, \overbrace{\nu^+, \dots, \nu^+}^{d_1}, \overbrace{\nu^-, \dots, \nu^-}^{d_2}), \\ \Sigma_{a_2} &= \text{diag}(\nu_0, \dots, \nu_0, \nu^-, \dots, \nu^-, \nu^+, \dots, \nu^+).\end{aligned}$$

An illustration with one replicate of each value is shown in Figure 1.

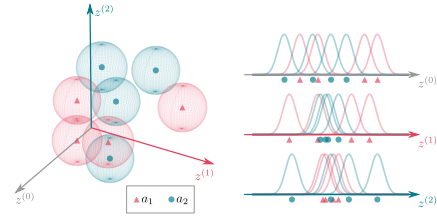


Figure 1: Illustration of the parametric model. Data points z are shown in three dimensions, with type a_1 represented by red triangles and type a_2 by green circles. Each class is best separated along specific axes: a_1 along the red ($z^{(1)}$) and a_2 along the green ($z^{(2)}$). On the axis $z^{(0)}$ both types can be separated, but not as effectively as on their respective optimal axes.

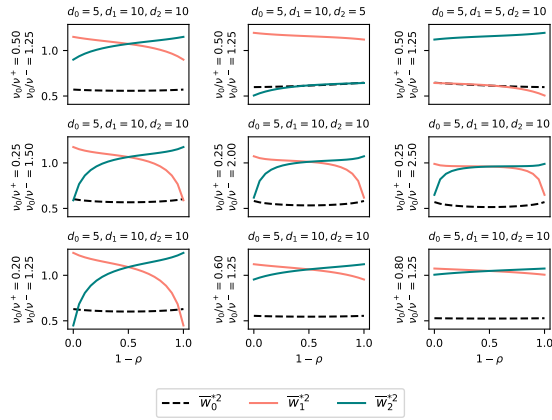


Figure 2: Optimal weight values for varying variance and dimension ratios, as a function of ρ .

The following proposition shows that if the number of components d_2 corresponding to ν^- for the training classes is not too large, that is $d_2 < h(\rho, \nu_z, \nu_0, \nu_1, \nu_2 d_1)$, the optimal solution for the training distribution prioritizes the components (features) corresponding to ν^+ for classes of type a_1 . Note that if d_2 is large, when combined, the corresponding components may still provide reasonable separation. We define h in equation 35, and provide the proof of Proposition 1 in Appendix B.2.

Proposition 1. Consider a weight representation $g(z) = Wz$, where $W \in \mathbb{R}^{d \times d}$ is a diagonal matrix $W = \text{diag}(w)$, and the squared Euclidean distance $d_g(z_i, z_j) = \|W(z_i - z_j)\|^2$. Let $W^* = \text{diag}(w^*)$ be such that $W^* \in \arg \min_W \mathbb{E} [\tilde{\ell}(\cdot, \cdot, \cdot; d_g)]$. Denote $\bar{w}_1^{*2} = \frac{1}{d_1} \sum_{k=d_0+1}^{d_1} w_k^*$ and $\bar{w}_2^{*2} = \frac{1}{d_2} \sum_{k=d_1+1}^d w_k^*$. Then for all $\rho > \frac{1}{2}$, and $\nu_z, \nu_0, \nu_1, \nu_2, d_1, d_2$ satisfying $d_2 < h(\rho, \nu_z, \nu_0, \nu_1, \nu_2, d_1)$ we have $d_2 \bar{w}_2^{*2} \leq d_1 \bar{w}_1^{*2}$.

Since components corresponding to ν^+ for classes of type a_1 align with ν^- for classes of type a_2 , the optimal representation on the training distribution yields poor separation on the shifted test distribution. Therefore, a robust representation should prioritize dimensions that provide effective separation for both class types, corresponding to ν_0 .

In Appendix B.3 we provide the full analytical solution w^* that minimizes the expected loss $\mathbb{E} [\tilde{\ell}(\cdot, \cdot, \cdot; d_g)]$ or the weight representation $g(z) = Wz$, using the squared Euclidean distance. According to Proposition 1, larger d_2 values favor ν^- for better aggregated separation. Increasing ν_0/ν^+ leads to growing differences between w_1^{*2} and w_2^{*2} , and vice versa for ν_0/ν^- .

This aligns with a common consideration in the Out-of-Distribution (OOD) generalization field (see §2), often referred to as *invariance*.

4 Proposed Approach

Motivated by the analysis of the parametric model we propose a new approach to tackle class distribution shifts in zero-shot learning. Our approach revolves around two key ideas: (i) during training, different mixtures of the attribute A can be achieved through sampling of small subsets of the classes, and (ii) penalizing for differences in performance across these environments is likely to increase robustness to the class mixture encountered at testing.

4.1 Synthetic Environments

Standard ERM training involves sampling pairs of data points (z_i, z_j) uniformly at random from all N_c classes available during training. However, as discussed in §3, this is prone to overfitting to the training attribute mixture. Since the identity of the attribute is unknown, weighted sampling (and similar approaches) cannot be used to create environments with different attribute mixtures.

Yet, our goal is to design artificial environments with diverse compositions of the (unknown) attribute of interest. To do so we leverage the variability in small samples: while class subsets of similar size to N_c maintain attribute distributions similar to the overall training set, smaller subsets with $k \ll N_c$ classes are likely to exhibit distinct attribute distributions. Therefore, we propose creating multiple environments, composed of examples from a few sampled classes.

This results in a hierarchical sampling scheme for the data pairs: first, sample a subset of k classes, $S = \{c_1, \dots, c_k\}$. Then, for each $c \in S$ sample $2r$ pairs of data points as follows: r pairs from within the class c , $\{z_i; c_i = c\}$, uniformly at random (positive pairs); and r negative pairs, where one point is uniformly at random from c , and the other from all other data points in S , $\{z_i; c_i \neq c, c_i \in S\}$.¹

Across multiple class subsets $S = \{S_1, \dots, S_n\}$, this hierarchical sampling results in diverse mixtures of any unknown attribute (see Figure 3). In particular, in some of the class subsets, classes from the overall minority type form the majority within the environment.

4.2 Environment Balancing Algorithm for Class Distribution Shifts

Our goal is to learn data representations that will allow separation between classes without knowing which attribute is expected to change and how significantly. Therefore, we require the learned data representation to perform similarly well on all mixtures obtained on the synthetic environments.

¹Here for simplicity we create balanced environments, but different proportions of positive examples can be considered instead.

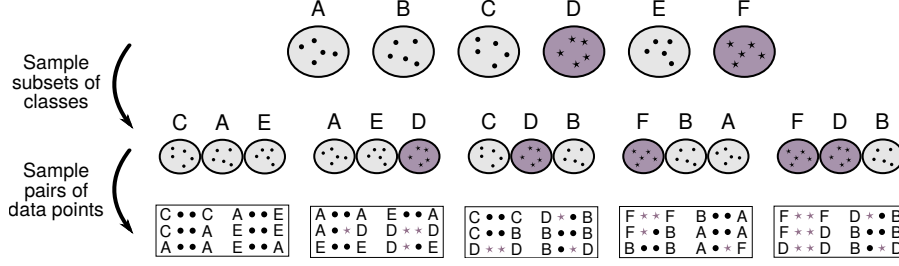


Figure 3: Illustration of the proposed hierarchical sampling. Top: $N_c = 6$ classes, with 2 minority-type classes D, F (in purple). Middle: synthetic environments formed by sampling small ($k = 3$) class sets – in $1/5$ of the environments, minority-type classes become the majority, constituting $2/3$ of the classes. Bottom: sampling $r = 1$ positive and $r = 1$ negative pairs for each class in the environment.

To achieve this, inspired by performance balancing methods in OOD (see §2) we optimize a penalized objective:

$$\min_{\theta} \sum_{l=1}^n \ell^{S_l}(g_{\theta}) + \lambda R(S_1, \dots, S_n) \quad (6)$$

where $R(S_1, \dots, S_n)$ is any balancing term across the constructed synthetic environments.

Note that computing $R(S_1, \dots, S_n)$ often involves evaluating some value on each environment separately. For a general balancing term, we denote the value in the l -th environment as $f(S_l)$, and accordingly express $R(S_1, \dots, S_n) = \mathring{f}(f(S_1), \dots, f(S_n))$, where \mathring{f} represents the corresponding aggregation function. Our combined approach², which entails balancing performance over synthetic environments of class subsamples, is outlined in Algorithm 1.

Algorithm 1 Robust Zero-Shot Representation

Input: Labeled data $D = \{z_i, c_i\}_{i=1}^{N_z}$, number of synthetic environments n , number of classes within subset k , number of pairs per class $2r$, neural network $g(\cdot; \theta)$, loss ℓ , distance function d , regularization functions f, \mathring{f} , initial weights θ_0 , number of training iterations T , learning rate η

Output: Learned representation $g(\cdot; \theta_T)$

Compute unique classes $C^* = \{c^{(1)}, \dots, c^{(N_c)}\}$

for $t = 1$ **to** T **do**

for $l = 1$ **to** n **do**

 Sample k classes from C^* without replacement: $S_l^{(t)} = \{c_l^{(1)}, \dots, c_l^{(k)}\}$

 From each class in $S_l^{(t)}$ sample r positive and r negative data pairs. Denote the set by $D_l^{(t)}$.

 Compute $f(S_l^{(t)})$.

 Compute average unpenalized loss over $(x_m, y_m) \in D_l^{(t)}$: $\bar{\ell}_l^{(t)} = \frac{1}{2rk} \sum_{m=1}^{2rk} \ell(x_m, y_m)$.

end for

 Compute $R^{(t)} := R(S_1^{(t)}, \dots, S_n^{(t)}) = \mathring{f}(f(S_1^{(t)}), \dots, f(S_n^{(t)}))$

 Update network parameters performing a gradient descent step:

$\theta^{(t)} \leftarrow \theta^{(t-1)} - \eta \nabla_{\theta} \left(\frac{1}{n} \sum_{l=1}^n \bar{\ell}_l^{(t)} + R^{(t)} \right)$

end for

Return: $g(\cdot; \theta_T)$

4.3 Balancing Performance Instead of Loss

In numerous OOD penalties, such as IRM and VarREx, f is the loss in each environment, which is distance-based in deep metric learning algorithms. This presents a challenge in zero-shot verification,

²For notation simplicity we assume the unpenalized training loss is applied to pairs of data points $(x_{ij}, y_{ij}) = ((z_i, z_j), \mathbb{1}_{c_i=c_j})$, but it can be easily adapted for any tuple size (e.g., triplets).

where sampled tuples often include numerous easy negative examples, leading to quick performance plateaus, despite considerable variations in distances themselves. Strategies like selecting the most difficult tuples [18] were proposed to address this issue. However, these methods have been observed to generate noisy gradients and loss values [34].

We therefore propose to directly balance performance instead of relying on the losses in the training environments. Denote the set of negative pairs within a synthetic environment by $D_l^0 = \{x_{ij} = (z_i, z_j) : c_i, c_j \in S_l, y_{ij} = 0\}$, and the set of positive pairs by $D_l^1 = \{x_{ij} = (z_i, z_j) : c_i, c_j \in S_l, y_{ij} = 1\}$. An unbiased estimator of the AUC on a given synthetic environment S_l is given by

$$\widehat{\text{AUC}}(S_l; d_g) = \frac{1}{|D_l^0| |D_l^1|} \sum_{x_{ij} \in D_l^0} \sum_{x_{uv} \in D_l^1} \mathbb{1}[d_g(x_{ij}) < d_g(x_{uv})] \quad (7)$$

for $x_{ij} \in D_l^1$ and $x_{uv} \in D_l^0$. Since this estimator is non-differentiable, and therefore cannot be used in gradient-descent based optimization, we use an approximation named *soft-AUC* [7]

$$\widehat{\text{AUC}}(S_l; d_g) \approx \frac{1}{|D_l^0| |D_l^1|} \sum_{x_{ij} \in D_l^0} \sum_{x_{uv} \in D_l^1} \sigma_\beta(d_g(x_{uv}) - d_g(x_{ij})) \quad (8)$$

where a sigmoid $\sigma_\beta(t) = \frac{1}{1+e^{-\beta t}}$ approximates the step function. Note that when $\beta \rightarrow \infty$, σ_β converges pointwise to the step function. Consequently, we propose the penalty:

$$R_{\text{VarAUC}}(S_1, \dots, S_n; g_d) = \widehat{\text{Var}}\left(\widehat{\text{AUC}}(S_1; g, d), \dots, \widehat{\text{AUC}}(S_n; g, d)\right). \quad (9)$$

4.4 How Many Environments are Needed?

The proposed hierarchical sampling allows for the construction of many synthetic environments with various attribute mixtures, influenced by the number of classes in each environment. As shown in the subsequent analysis, this ensures that, with high probability, classes with rare attribute values will appear together in the same environment. This, in turn, facilitates learning to separate negative pairs involving rare class types.

At each training iteration, we consider n class subsets (environments) of size k . Our goal is to achieve robustness to all attribute values a that are associated with at least $\rho_{\min} \in (0, 1)$ of the training classes. Note that ρ_{\min} is specified by the practitioner without knowledge of the true attribute that may cause the shift, or its true abundance ρ in the training set.

We compute the number of synthetic environments n , such that with high probability of $(1 - \alpha)$, S_1, \dots, S_n will include at least one subset with at least two classes associated with a (otherwise none of the subsets would contain negative pairs with the attribute a). Denote the probability of a given subset to not contain any class associated with a by $\phi_0 = \left(\frac{(1-\rho_{\min})^{N_c}}{k}\right) / \binom{N_c}{k}$, and the probability of a given subset to contain exactly one such class by $\phi_1 = \frac{\rho_{\min} N_c \left(\frac{(1-\rho_{\min})^{N_c}}{k-1}\right)}{\binom{N_c}{k}}$. This corresponds to n that is typically much smaller than $\binom{N_c}{k}$, given by $n \approx \frac{\log(\alpha)}{\log(\phi_0 + \phi_1)} \cdot (10)$

5 Empirical Results

Our method enhances standard training with two components: hierarchical sub-sampling and a balancing term for synthetic environments. To our knowledge, this is the first work addressing OOD generalization for class distribution and zero-shot learning. We therefore benchmark our algorithm against the ERM baseline (uniform random sampling with an unpenalized score) and optimization of an unpenalized score over hierarchical samples, providing an ablation study. Additionally, we tested standard regularization techniques such as dropout and the L_2 norm, which did not yield notable improvements in the distribution shift scenario, and therefore are not shown.

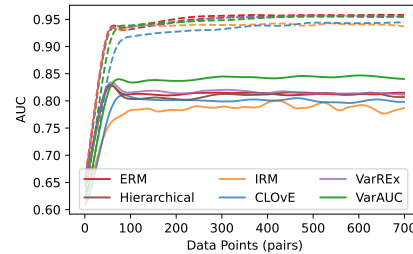


Figure 4: Average AUC over 10 simulation repetitions for $\rho = 0.9$. Solid lines: distribution-shift. Dashed lines: in-distribution. Our method improves robustness for shifts, without compromising training distribution results.

For comprehensive comparisons, in addition to the proposed VarAUC penalty, we evaluate variants of our algorithm with IRM, CLOvE, and VarREx penalties as well. While we show that VarAUC consistently outperforms other penalties, the crucial improvement lies in its performance compared to the ERM baseline: application of existing OOD penalties is enabled by the construction of synthetic environments in our framework. As discussed in Appendix C, this construction facilitates the formulation of previously untreated class distribution shifts in zero-shot learning within the OOD setting.

Across all experiments, we trained the network with contrastive loss (Equation 2) and normalized cosine distance: $d_g(z_1, z_2) = \frac{1}{2} \left(1 - \frac{g(z_1) \cdot g(z_2)}{\|g(z_1)\| \|g(z_2)\|} \right)$. The exact setups are detailed below and additional details appear in Appendix F.

5.1 Simulations: Revisiting the Parametric Model

Here we revisit the parametric model presented in §3. To increase the complexity of the problem we add dimensions where classes from both types are not well separated. That is, Σ_a includes additional dimensions set to zero.

Setup We used 68 subsets in each training iteration, each consisting of two classes. This corresponds to choosing $\rho_{\min} = 0.1$ (desired sensitivity, regardless of the true unknown parameter $\rho \in \{0.05, 0.1, 0.3\}$) with a low α value of 0.5, resulting in the construction of fewer environments according to Equation 4.4. For each class, we sampled $2r = 10$ pairs of data points. The representation was defined as $g(z) = wz$ for $w \in \mathbb{R}^{d \times p}$ ³. Here we focus on the case of $p = 16$, $\nu_z = \nu_0 = 1$, $\nu^- = 0.1$, $\nu_+ = 2$, $d_0 = 5$, $d_1 = d_2 = 10$. Additional representation sizes p , noise ratios $\frac{\nu^+}{\nu^-}$ and varying proportions of positive and negative examples are shown in Appendix D.1.

To assess the importance assigned to each dimension, we examine weight values relative to other weights: $\text{Importance}_i = \left| \frac{\sum_{j=1}^p w_{ij}}{\sum_{i'=1}^d \sum_{j'=1}^p w_{i'j'}} \right|$. (11)

Results In Figure 5 we examine the learned representation. The analysis reveals that ERM prioritizes dimensions 5-15, providing good separation for a_1 , the dominant type in training, but leading to poor separation after the shift. ERM assigns low weights to dimensions beneficial for both types (0-5) and those suitable for a_2 (15-25). In contrast, our algorithm, particularly with the two variance-based penalties, assigns the lowest weights to dimensions corresponding to a_1 and higher weights to shared dimensions and those that effectively separate a_2 classes.

In Figure 4, the learning progress is depicted for $\rho = 0.9$, and similar analysis for $\rho = 0.95$ and $\rho = 0.7$ can be found in Appendix D. Performance on the same distribution as the training data is similar between ERM and our algorithm, suggesting that applying our algorithm does not negatively impact performance when no distribution shift occurs. However, under distribution shift our algorithm achieves much better results. The VarREx penalty achieves high AUC values more quickly than the VarAUC penalty, but VarAUC attains higher accuracy overall. IRM shows noisier convergence since it is applied directly on the gradients, which have been shown to be noisy in contrastive learning due to high variance in data-pair samples [34]. Means and standard deviations are reported in Appendix D.1, as well as results for additional data dimensions, positive proportions and variance ratios.

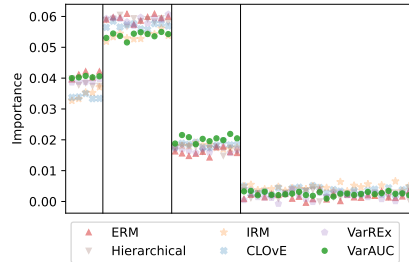


Figure 5: Avg. feature importance for $\rho = 0.9$, 10 repetitions. Our VarAUC method emphasizes shared features (blocks 1 and 3) most, while de-prioritizing majority features (block 2). All methods assign low weight to noise features (block 4).

5.2 Experiments on Real Data

Experiment 1 - Face Recognition We used the *CelebA* dataset [30] that contains 202,599 images of 10,177 celebrities. We filtered out people for who less than 3 images were present. Following Vinyals

³A linear representation is chosen to facilitate an analysis of the learned representation space.

et al. [51] we implemented g as a convolutional neural network which has 4 modules with 3×3 convolutions and 64 filters, followed by batch normalization, a ReLU activation, 2×2 max-pooling and a fully connected layer of size 32 . We used the attribute *blond hair* for the class distribution shift: for training we sampled mostly non-blond people (95%) while in test most people (95%) were blond. Training iteration had 150 synthetic environments of 2 classes and $2r = 20$ data points per class.

Experiment 2 - Species Recognition We used the ETHEC dataset [11] which includes 47,978 butterfly images from 6 families and 561 species (example images are provided in Appendix D). We filtered out species with less than 5 images and focused on images of butterflies from the Lycaenidae and Nymphalidae families. We included in the training set 10% of species from the Nymphalidae family, while at test time 90% of the species were from the Nymphalidae family. For each class we sampled $2r = 20$ pairs. We trained the models on 200 synthetic environments at a time, each of two classes. We implemented g as a fully connected neural network with layers of sizes 128, 64, 32 and 16, and ReLU activations between them.

Experimental Results Figure 6 shows that all versions of our algorithm achieve some improvement over ERM, where best results are achieved with VarAUC penalty. Exact means and standard deviations are reported in Table 3 in the Appendix. One-sided paired t-tests show that the improvement over ERM achieved by our algorithm with the VarAUC penalty is statistically significant, with p-values of < 0.04 on both datasets. p-values for other penalties are reported in Table 4. All p-values were adjusted with FDR [4] correction.

In Appendix D we provide additional analysis confirming that the main improvement of our algorithm over the ERM baseline stems from improved performance on negative minority pairs.

6 Discussion

In this study, we examined class distribution shifts in zero-shot learning, with a focus on shifts induced by unknown attributes. Such shifts pose significant challenges in zero-shot learning, where new classes emerge in testing, causing standard techniques trained via ERM to fail on shifted class distributions, even when the conditional distribution of the data given the class remains the same.

Existing lines of work (see Appendix A) assumes closed-world classification or a known cause, making it unsuitable for zero-shot learning or shifts caused by unknown attributes. In response, we introduced a straightforward framework and the first algorithm to address class distribution shifts in zero-shot learning using OOD environment balancing methods.

In the causal terminology of closed-world OOD generalization, our framework employs synthetic environments to intervene on attribute mixtures by sampling small class subsets, thereby manipulating the class distribution. This facilitates the creation of diverse environments with varied attribute mixtures, enhancing the distinction between negative examples. We further discuss the comparison with OOD balancing methods in Appendix C. Additionally, our proposed VarAUC penalty, designed for metric losses, enhances the separation of negative examples.

Our results demonstrate improvements compared to the ERM baseline on shifted distributions without compromising performance on unshifted ones, enabling the learning of more robust representations for zero-shot tasks and ensuring reliable performance.

While the proposed framework is general, our current experiments address shifts in a binary attribute. We defer exploration of additional scenarios, such as those involving shifts in multiple correlated attributes, to future work. An additional promising direction for future work is the consideration of shifts where the responsible attribute is strongly correlated with additional attributes or covariates. This opens possibilities to explore structured constructions of synthetic environments that leverages such correlations.

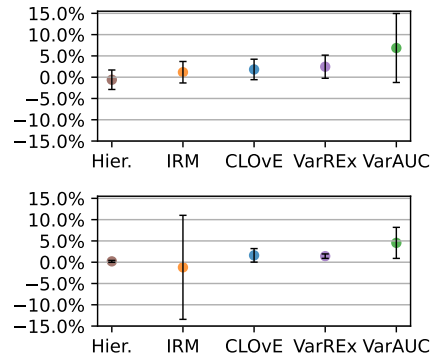


Figure 6: Average percentage changes across 10 repetitions compared to ERM are shown for the ETHEC (top) and CelebA (bottom) datasets. Error bars represent \pm one std-dev.

References

- [1] Martin Arjovsky, Léon Bottou, Ishaan Gulrajani, and David Lopez-Paz. Invariant risk minimization. *arXiv preprint arXiv:1907.02893*, 2019.
- [2] Tadas Baltrusaitis, Amir Zadeh, Yao Chong Lim, and Louis-Philippe Morency. Openface 2.0: Facial behavior analysis toolkit. In *2018 13th IEEE international conference on automatic face & gesture recognition (FG 2018)*, pages 59–66. IEEE, 2018.
- [3] Aharon Ben-Tal, Dick Den Hertog, Anja De Waegenare, Bertrand Melenberg, and Gijs Rennen. Robust solutions of optimization problems affected by uncertain probabilities. *Management Science*, 59(2):341–357, 2013.
- [4] Yoav Benjamini and Yosef Hochberg. Controlling the false discovery rate: a practical and powerful approach to multiple testing. *Journal of the Royal statistical society: series B (Methodological)*, 57(1):289–300, 1995.
- [5] Lacey Best-Rowden and Anil K Jain. Longitudinal study of automatic face recognition. *IEEE transactions on pattern analysis and machine intelligence*, 40(1):148–162, 2017.
- [6] Jonathon Byrd and Zachary Lipton. What is the effect of importance weighting in deep learning? In *International conference on machine learning*, pages 872–881. PMLR, 2019.
- [7] Toon Calders and Szymon Jaroszewicz. Efficient auc optimization for classification. In *European conference on principles of data mining and knowledge discovery*, pages 42–53. Springer, 2007.
- [8] Kaidi Cao, Colin Wei, Adrien Gaidon, Nikos Arechiga, and Tengyu Ma. Learning imbalanced datasets with label-distribution-aware margin loss. *Advances in neural information processing systems*, 32, 2019.
- [9] Shiyu Chang, Yang Zhang, Mo Yu, and Tommi Jaakkola. Invariant rationalization. In *International Conference on Machine Learning*, pages 1448–1458. PMLR, 2020.
- [10] Yin Cui, Menglin Jia, Tsung-Yi Lin, Yang Song, and Serge Belongie. Class-balanced loss based on effective number of samples. In *Proceedings of the IEEE/CVF conference on computer vision and pattern recognition*, pages 9268–9277, 2019.
- [11] Ankit Dhall. Eth entomological collection (ethec) dataset [paleartic macrolepidoptera, spring 2019]. 2019.
- [12] John C Duchi and Hongseok Namkoong. Learning models with uniform performance via distributionally robust optimization. *The Annals of Statistics*, 49(3):1378–1406, 2021.
- [13] John C Duchi, Peter W Glynn, and Hongseok Namkoong. Statistics of robust optimization: A generalized empirical likelihood approach. *Mathematics of Operations Research*, 46(3): 946–969, 2021.
- [14] Li Fei-Fei, Rob Fergus, and Pietro Perona. One-shot learning of object categories. *IEEE transactions on pattern analysis and machine intelligence*, 28(4):594–611, 2006.
- [15] Patrick Grother, Mei Ngan, Kayee Hanaoka, et al. Ongoing face recognition vendor test (frvt) part 3: Demographic effects. *Nat. Inst. Stand. Technol., Gaithersburg, MA, USA, Rep. NISTIR*, 8280, 2019.
- [16] Zhangxuan Gu, Siyuan Zhou, Li Niu, Zihan Zhao, and Liqing Zhang. Context-aware feature generation for zero-shot semantic segmentation. In *Proceedings of the 28th ACM International Conference on Multimedia*, pages 1921–1929, 2020.
- [17] Raia Hadsell, Sumit Chopra, and Yann LeCun. Dimensionality reduction by learning an invariant mapping. In *2006 IEEE Computer Society Conference on Computer Vision and Pattern Recognition (CVPR’06)*, volume 2, pages 1735–1742. IEEE, 2006.
- [18] Alexander Hermans, Lucas Beyer, and Bastian Leibe. In defense of the triplet loss for person re-identification. *arXiv preprint arXiv:1703.07737*, 2017.

- [19] Alexander Hermans, Lucas Beyer, and Bastian Leibe. In defense of the triplet loss for person re-identification. *arXiv preprint arXiv:1703.07737*, 2017.
- [20] Elad Hoffer and Nir Ailon. Deep metric learning using triplet network. In *International workshop on similarity-based pattern recognition*, pages 84–92. Springer, 2015.
- [21] Badr Youbi Idrissi, Martin Arjovsky, Mohammad Pezeshki, and David Lopez-Paz. Simple data balancing achieves competitive worst-group-accuracy. In *Conference on Causal Learning and Reasoning*, pages 336–351. PMLR, 2022.
- [22] Aparna R Joshi, Xavier Suau Cuadros, Nivedha Sivakumar, Luca Zappella, and Nicholas Apostoloff. Fair sa: Sensitivity analysis for fairness in face recognition. In *Algorithmic fairness through the lens of causality and robustness workshop*, pages 40–58. PMLR, 2022.
- [23] Brendan F Klare, Mark J Burge, Joshua C Klontz, Richard W Vorder Bruegge, and Anil K Jain. Face recognition performance: Role of demographic information. *IEEE Transactions on information forensics and security*, 7(6):1789–1801, 2012.
- [24] Gregory Koch, Richard Zemel, Ruslan Salakhutdinov, et al. Siamese neural networks for one-shot image recognition. In *International Conference on Machine Learning (ICML) deep learning workshop*, volume 2, 2015.
- [25] David Krueger, Ethan Caballero, Joern-Henrik Jacobsen, Amy Zhang, Jonathan Binas, Dinghuai Zhang, Remi Le Priol, and Aaron Courville. Out-of-distribution generalization via risk extrapolation (rex). In *International Conference on Machine Learning*, pages 5815–5826. PMLR, 2021.
- [26] Aviral Kumar, Sunita Sarawagi, and Ujjwal Jain. Trainable calibration measures for neural networks from kernel mean embeddings. In Jennifer Dy and Andreas Krause, editors, *Proceedings of the 35th International Conference on Machine Learning*, volume 80 of *Proceedings of Machine Learning Research*, pages 2805–2814. PMLR, 10–15 Jul 2018. URL <https://proceedings.mlr.press/v80/kumar18a.html>.
- [27] Hugo Larochelle, Dumitru Erhan, and Yoshua Bengio. Zero-data learning of new tasks. In *AAAI*, volume 1, page 3, 2008.
- [28] Tsung-Yi Lin, Priya Goyal, Ross Girshick, Kaiming He, and Piotr Dollár. Focal loss for dense object detection. In *Proceedings of the IEEE international conference on computer vision*, pages 2980–2988, 2017.
- [29] Evan Z Liu, Behzad Haghgoo, Annie S Chen, Aditi Raghunathan, Pang Wei Koh, Shiori Sagawa, Percy Liang, and Chelsea Finn. Just train twice: Improving group robustness without training group information. In *International Conference on Machine Learning*, pages 6781–6792. PMLR, 2021.
- [30] Ziwei Liu, Ping Luo, Xiaogang Wang, and Xiaoou Tang. Deep learning face attributes in the wild. In *Proceedings of International Conference on Computer Vision (ICCV)*, December 2015.
- [31] Arakaparampil M Mathai and Serge B Provost. Quadratic forms in random variables: theory and applications. (*No Title*), 1992.
- [32] Aditya Krishna Menon, Sadeep Jayasumana, Ankit Singh Rawat, Himanshu Jain, Andreas Veit, and Sanjiv Kumar. Long-tail learning via logit adjustment. In *International Conference on Learning Representations*, 2020.
- [33] Dana Michalski, Sau Yee Yiu, and Chris Malec. The impact of age and threshold variation on facial recognition algorithm performance using images of children. In *2018 International Conference on Biometrics (ICB)*, pages 217–224. IEEE, 2018.
- [34] Kevin Musgrave, Serge Belongie, and Ser-Nam Lim. A metric learning reality check. In *Computer Vision—ECCV 2020: 16th European Conference, Glasgow, UK, August 23–28, 2020, Proceedings, Part XXV 16*, pages 681–699. Springer, 2020.

- [35] Hyun Oh Song, Yu Xiang, Stefanie Jegelka, and Silvio Savarese. Deep metric learning via lifted structured feature embedding. In *Proceedings of the IEEE conference on computer vision and pattern recognition*, pages 4004–4012, 2016.
- [36] Jonas Peters, Peter Bühlmann, and Nicolai Meinshausen. Causal inference by using invariant prediction: identification and confidence intervals. *Journal of the Royal Statistical Society Series B: Statistical Methodology*, 78(5):947–1012, 2016.
- [37] Jonas Peters, Dominik Janzing, and Bernhard Schölkopf. *Elements of causal inference: foundations and learning algorithms*. The MIT Press, 2017.
- [38] Vihari Piratla, Praneeth Netrapalli, and Sunita Sarawagi. Focus on the common good: Group distributional robustness follows. In *International Conference on Learning Representations*, 2021.
- [39] Inioluwa Deborah Raji and Joy Buolamwini. Actionable auditing: Investigating the impact of publicly naming biased performance results of commercial ai products. In *Proceedings of the 2019 AAAI/ACM Conference on AI, Ethics, and Society*, pages 429–435, 2019.
- [40] Jiawei Ren, Cunjun Yu, Xiao Ma, Haiyu Zhao, Shuai Yi, et al. Balanced meta-softmax for long-tailed visual recognition. *Advances in neural information processing systems*, 33:4175–4186, 2020.
- [41] Joseph P Robinson, Gennady Livitz, Yann Henon, Can Qin, Yun Fu, and Samson Timoner. Face recognition: too bias, or not too bias? In *Proceedings of the IEEE/CVF Conference on Computer Vision and Pattern Recognition Workshops*, pages 0–1, 2020.
- [42] Mateo Rojas-Carulla, Bernhard Schölkopf, Richard Turner, and Jonas Peters. Invariant models for causal transfer learning. *The Journal of Machine Learning Research*, 19(1):1309–1342, 2018.
- [43] Karsten Roth, Timo Milbich, Samarth Sinha, Prateek Gupta, Bjorn Ommer, and Joseph Paul Cohen. Revisiting training strategies and generalization performance in deep metric learning. In *International Conference on Machine Learning*, pages 8242–8252. PMLR, 2020.
- [44] Marco Saerens, Patrice Latinne, and Christine Decaestecker. Adjusting the outputs of a classifier to new a priori probabilities: a simple procedure. *Neural computation*, 14(1):21–41, 2002.
- [45] Shiori Sagawa, Pang Wei Koh, Tatsunori B Hashimoto, and Percy Liang. Distributionally robust neural networks. In *International Conference on Learning Representations*, 2019.
- [46] Hidetoshi Shimodaira. Improving predictive inference under covariate shift by weighting the log-likelihood function. *Journal of statistical planning and inference*, 90(2):227–244, 2000.
- [47] Tomáš Sixta, Julio CS Jacques Junior, Pau Buch-Cardona, Eduard Vazquez, and Sergio Escalera. Fairface challenge at eccv 2020: Analyzing bias in face recognition. In *Computer Vision–ECCV 2020 Workshops: Glasgow, UK, August 23–28, 2020, Proceedings, Part VI 16*, pages 463–481. Springer, 2020.
- [48] Yuli Slavutsky and Yuval Benjamini. Predicting classification accuracy when adding new unobserved classes. In *International Conference on Learning Representations, ICLR, Conference Track Proceedings*, 2021.
- [49] Kihyuk Sohn. Improved deep metric learning with multi-class n-pair loss objective. *Advances in neural information processing systems*, 29, 2016.
- [50] Nisha Srinivas, Karl Ricanek, Dana Michalski, David S Bolme, and Michael King. Face recognition algorithm bias: Performance differences on images of children and adults. In *Proceedings of the IEEE/CVF conference on computer vision and pattern recognition workshops*, pages 0–0, 2019.
- [51] Oriol Vinyals, Charles Blundell, Timothy Lillicrap, Daan Wierstra, et al. Matching networks for one shot learning. *Advances in neural information processing systems*, 29, 2016.

- [52] Yoav Wald, Amir Feder, Daniel Greenfeld, and Uri Shalit. On calibration and out-of-domain generalization. *Advances in neural information processing systems*, 34:2215–2227, 2021.
- [53] Mei Wang and Weihong Deng. Mitigating bias in face recognition using skewness-aware reinforcement learning. In *Proceedings of the IEEE/CVF conference on computer vision and pattern recognition*, pages 9322–9331, 2020.
- [54] Mei Wang, Weihong Deng, Jiani Hu, Xunqiang Tao, and Yaohai Huang. Racial faces in the wild: Reducing racial bias by information maximization adaptation network. In *Proceedings of the IEEE/CVF international conference on computer vision*, pages 692–702, 2019.
- [55] Jiaheng Wei, Harikrishna Narasimhan, Ehsan Amid, Wen-Sheng Chu, Yang Liu, and Abhishek Kumar. Distributionally robust post-hoc classifiers under prior shifts. In *International Conference on Learning Representations (ICLR)*, 2023.
- [56] Chao-Yuan Wu, R Manmatha, Alexander J Smola, and Philipp Krahenbuhl. Sampling matters in deep embedding learning. In *Proceedings of the IEEE international conference on computer vision*, pages 2840–2848, 2017.
- [57] Yongqin Xian, Subhabrata Choudhury, Yang He, Bernt Schiele, and Zeynep Akata. Semantic projection network for zero-and few-label semantic segmentation. In *Proceedings of the IEEE/CVF Conference on Computer Vision and Pattern Recognition*, pages 8256–8265, 2019.
- [58] Tongtong Yuan, Weihong Deng, Jian Tang, Yinan Tang, and Binghui Chen. Signal-to-noise ratio: A robust distance metric for deep metric learning. In *Proceedings of the IEEE/CVF conference on computer vision and pattern recognition*, pages 4815–4824, 2019.
- [59] Charles Zheng, Rakesh Achanta, and Yuval Benjamini. Extrapolating expected accuracies for large multi-class problems. *The Journal of Machine Learning Research*, 19(1):2609–2638, 2018.
- [60] Zhisheng Zhong, Jiequan Cui, Shu Liu, and Jiaya Jia. Improving calibration for long-tailed recognition. In *Proceedings of the IEEE/CVF conference on computer vision and pattern recognition*, pages 16489–16498, 2021.

A Related Work on Class Distribution Shifts in Closed-World Settings

In *Class-Imbalanced Learning* [28, 10, 8] it is assumed that some classes are more dominant in training, while in deployment this is no longer the case. Therefore, solutions classically include data or loss re-weighting [46, 6, 40, 32] and calibration of the classification score [44, 60]. A particularly popular framework to address class distribution shifts is *Distributionally Robust Optimization* (DRO) [3, 13, 12, 55], where instead of assuming a specific probability distribution, a set or a range of possible distributions is considered, and optimization is performed to achieve best results over the worst-case distribution. A special case known as *Group DRO* [45, 38], involves a group variable that introduces discriminatory patterns among classes within specific groups. This framework includes methods that assume that the classifier does not have access to the group information, and therefore propose re-weighting high loss examples [29], and data sub-sampling to balance classes and groups [21]. Nevertheless, all these methodologies rely on the training and test class sets being identical, making them unsuitable for direct application in zero-shot learning scenarios.

B Analysis of the Parametric Model

B.1 Derivation of the Loss

We begin by revisiting the parametric model introduced in §3. Let $z_i|c_i \sim \mathcal{N}(c_i, \Sigma_z)$, where $\Sigma_z = \nu_z I_d$, $0 < \nu_z \in \mathbb{R}$ and I_d is the d dimensional identity matrix. Classes c_i are drawn according to a Gaussian distribution $c_i \sim \mathcal{N}(0, \Sigma_a)$ corresponding to their type $a \in \{a_1, a_2\}$. Here, we use a simpler (although less intuitive) notation for the values of the diagonal matrices Σ_a :

$$\begin{aligned}\Sigma_{a_1} &= \text{diag}(\overbrace{\nu_0, \dots, \nu_0}^{d_0}, \overbrace{\nu_1, \dots, \nu_1}^{d_1}, \overbrace{\nu_2, \dots, \nu_2}^{d_2}), \\ \Sigma_{a_2} &= \text{diag}(\nu_0, \dots, \nu_0, \nu_2, \dots, \nu_2, \nu_1, \dots, \nu_1),\end{aligned}$$

where $0 < \nu_2 < \nu_z < \nu_0 < \nu_1$.

We consider a weight representations $g(z) = Wz$, where W is a diagonal matrix with diagonal $w \in \mathbb{R}^d$.

Since Σ_z is of full rank, it suffices to consider the no-Hinge version of the contrastive loss, that is

$$\tilde{\ell}(z_i, z_j, y_{ij}; d_g) := y_{ij} \|W(z_i - z_j)\|^4 + (1 - y_{ij}) \left(m - \|W(z_i - z_j)\|^2\right)^2, \quad (12)$$

where $d_g(z_i, z_j) := \|g(z_i - z_j)\|^2 = \|W(z_i - z_j)\|^2$ ($\|\cdot\|$ denotes the Euclidean norm⁴).

For a balanced sample of positive and negative examples, the expected loss is given by

$$\begin{aligned}\mathbb{E}[\tilde{\ell}(z_i, z_j, y_{ij}; d_g)] &= \frac{1}{2} \mathbb{E}_{y_{ij}=1} [\|W(z_i - z_j)\|^4] \\ &\quad + \frac{1}{2} \mathbb{E}_{y_{ij}=0} [m^2 - 2m \|W(z_i - z_j)\|^2 + \|W(z_i - z_j)\|^4].\end{aligned} \quad (13)$$

To calculate the expression above, we begin by proving the following lemma:

Lemma 1. *Let $\mu \in \mathbb{R}^d$ be a random variable and let $t|\mu \sim \mathcal{N}(\mu, \Sigma)$. If $\mu \equiv 0$ (constant), then*

$$1. \quad \mathbb{E} \|t\|^4 = 2 \text{tr}(\Sigma^2) + \text{tr}^2(\Sigma).$$

If $\mu \sim \mathcal{N}(0, \Sigma_\mu)$, then

$$2. \quad \mathbb{E} \|t\|^2 = \text{tr}(\Sigma) + \text{tr}(\Sigma_\mu),$$

$$3. \quad \mathbb{E} \|t\|^4 = 2 \text{tr}(\Sigma^2) + 4 \text{tr}(\Sigma \Sigma_\mu) + \text{tr}^2(\Sigma) + 2 \text{tr}(\Sigma) \text{tr}(\Sigma_\mu) + 2 \text{tr}(\Sigma_\mu^2) + \text{tr}^2(\Sigma_\mu).$$

⁴Squared distance is selected for its simplicity in computing the expected value of even powers of the Euclidean norm of Gaussian variables.

Proof. For any random variable $u \in \mathbb{R}^d$, such that $u \sim \mathcal{N}(\mu_u, \Sigma_u)$, and any symmetric matrix A , we have

$$\mathbb{E}_u[u^T A u] = \text{tr}(A \Sigma_u) + \mu_u^T A \mu_u, \quad (14)$$

$$\mathbb{E}_u[u^T A u]^2 = 2 \text{tr}((A \Sigma_u)^2) + 4 \mu_u^T A \Sigma_u A \mu_u + (\text{tr}(A \Sigma_u) + \mu_u^T A \mu_u)^2 \quad (15)$$

(see, for example, Thm. 3.2b.2 in [31]).

First, letting $\mu_u = 0$, $\Sigma_u = \Sigma$ and $A = I_d$ in (15) we get

$$\mathbb{E} \|t\|^4 = \mathbb{E}[t^T t]^2 = 2 \text{tr}(\Sigma^2) + \text{tr}^2(\Sigma). \quad (16)$$

Now, assume that $\mu \sim \mathcal{N}(0, \Sigma_\mu)$. From (14) we get $\mathbb{E}_\mu \|\mu\|^2 = \mathbb{E}_\mu[\mu^T \mu] = \text{tr}(\Sigma_\mu)$, and thus

$$\mathbb{E} \|t\|^2 = \mathbb{E}_\mu [\mathbb{E}_{t|\mu}[t^T t | \mu]] = \mathbb{E}_\mu [\text{tr}(\Sigma) + \mu^T \mu] = \text{tr}(\Sigma) + \text{tr}(\Sigma_\mu). \quad (17)$$

Similarly, from (15) we have

$$\mathbb{E} \|t\|^4 = \mathbb{E}_\mu [\mathbb{E}_{t|\mu}[t^T t]^2 | \mu]] = 2 \text{tr}(\Sigma^2) + 4 \mathbb{E}_\mu[\mu^T \Sigma \mu] + \text{tr}^2(\Sigma) + 2 \text{tr}(\Sigma) \mathbb{E}_\mu \|\mu\|^2 + \mathbb{E}_\mu \|\mu\|^4. \quad (18)$$

By substituting $A = \Sigma$ in (14) we get $\mathbb{E}_\mu[\mu^T \Sigma \mu] = \text{tr}(\Sigma \Sigma_\mu)$, and from (15) we have

$$\mathbb{E}_\mu \|\mu\|^4 = 2 \text{tr}(\Sigma_\mu^2) + \text{tr}^2(\Sigma_\mu). \quad (19)$$

Therefore,

$$\mathbb{E} \|t\|^4 = 2 \text{tr}(\Sigma^2) + 4 \text{tr}(\Sigma \Sigma_\mu) + \text{tr}^2(\Sigma) + 2 \text{tr}(\Sigma) \text{tr}(\Sigma_\mu) + 2 \text{tr}(\Sigma_\mu^2) + \text{tr}^2(\Sigma_\mu). \quad (20)$$

□

Note that $W(z_i - z_j) \sim \mathcal{N}(\mu, \Sigma)$, with $\mu = W(c_i - c_j)$ and $\Sigma = 2\nu_z W^T W$.

If $y_{ij} = 1$, then z_i and z_j are from the same class, meaning that $c_i = c_j$ and thus $\mu = 0$. Therefore, by Lemma 1.(1) we have

$$\begin{aligned} \mathbb{E}_{y_{ij}=1} \|W(z_i - z_j)\|^4 &= 2 \text{tr}(\Sigma^2) + \text{tr}^2(\Sigma) \\ &= 2 \cdot 4\nu_z^2 \text{tr}([W^T W]^2) + 4\nu_z^2 \text{tr}^2(W^T W) \\ &= 8\nu_z^2 \sum_{i=1}^d w_i^4 + 4\nu_z^2 \left(\sum_{i=1}^d w_i^2 \right)^2. \end{aligned} \quad (21)$$

However, for pairs from different classes, that is, when $y_{ij} = 0$, the mean μ is itself a Gaussian random variable distributed according to $\mathcal{N}(0, \Sigma_\mu)$, where

$$\Sigma_\mu = \begin{cases} W^T (2\Sigma_{a_1}) W & c_i, c_j \text{ are both of type } a_1 \\ W^T (2\Sigma_{a_2}) W & c_i, c_j \text{ are both of type } a_2 \\ W^T (\Sigma_{a_1} + \Sigma_{a_2}) W & c_i, c_j \text{ are of different types.} \end{cases} \quad (22)$$

Therefore, by Lemma 1.(2) we have

$$\begin{aligned} \mathbb{E}_{y_{ij}=0} \|W(z_i - z_j)\|^2 &= \mathbb{E}_{y_{ij}=0} [\text{tr}(\Sigma_\mu) + \text{tr}(\Sigma)] = \mathbb{E}_{y_{ij}=0} [\text{tr}(\Sigma_\mu)] + \text{tr}(\Sigma) \\ &= \rho^2 \text{tr}(2W^T \Sigma_{a_1} W) + (1 - \rho)^2 \text{tr}(2W^T \Sigma_{a_2} W) \\ &\quad + 2\rho(1 - \rho) \text{tr}(W^T (\Sigma_{a_1} + \Sigma_{a_2}) W) + \text{tr}(\Sigma) \\ &= 2 \left[(\nu_0 + \nu_z) \sum_{i=1}^{d_0} w_i^2 + (\alpha_1 + \nu_z) \sum_{i=d_0+1}^{d_0+d_1} w_i^2 + (\alpha_2 + \nu_z) \sum_{i=d_0+d_1+1}^d w_i^2 \right], \end{aligned} \quad (23)$$

where

$$\begin{aligned}
\alpha_1 &:= \rho^2 \nu_1 + (1 - \rho)^2 \nu_2 + \rho(1 - \rho)(\nu_1 + \nu_2) = \rho \nu_1 + (1 - \rho) \nu_2, \\
\alpha_2 &:= \rho^2 \nu_2 + (1 - \rho)^2 \nu_1 + \rho(1 - \rho)(\nu_1 + \nu_2) = \rho \nu_2 + (1 - \rho) \nu_1, \\
\beta_1 &:= 2\rho^2 \nu_1^2 + 2(1 - \rho)^2 \nu_2^2 + \rho(1 - \rho)(\nu_1 + \nu_2)^2, \\
\beta_2 &:= 2\rho^2 \nu_2^2 + 2(1 - \rho)^2 \nu_1^2 + \rho(1 - \rho)(\nu_1 + \nu_2)^2.
\end{aligned} \tag{24}$$

By Lemma 1.(3) we have

$$\begin{aligned}
\mathbb{E}_{y_{ij}=0} \|w(z_i - z_j)\|^4 &= \mathbb{E}_{y_{ij}=0} \left[2 \operatorname{tr}(\Sigma^2) + 4 \operatorname{tr}(\Sigma \Sigma_\mu) + \operatorname{tr}^2(\Sigma) + 2 \operatorname{tr}(\Sigma) \operatorname{tr}(\Sigma_\mu) + 2 \operatorname{tr}(\Sigma_\mu^2) + (\operatorname{tr}(\Sigma_\mu))^2 \right] \\
&= 2 \operatorname{tr}(\Sigma^2) + 4 \mathbb{E}_{y_{ij}=0} [\operatorname{tr}(\Sigma \Sigma_\mu)] + \operatorname{tr}^2(\Sigma) + 2 \operatorname{tr}(\Sigma) \mathbb{E}_{y_{ij}=0} [\operatorname{tr}(\Sigma_\mu)] \\
&\quad + 2 \mathbb{E}_{y_{ij}=0} [\operatorname{tr}(\Sigma_\mu^2)] + \mathbb{E}_{y_{ij}=0} [\operatorname{tr}^2(\Sigma_\mu)],
\end{aligned} \tag{25}$$

where

$$\begin{aligned}
\mathbb{E}_{y_{ij}=0} [\operatorname{tr}(\Sigma \Sigma_\mu)] &= 2\nu_z \operatorname{tr}(W^T W [2\rho^2 W^T \Sigma_{a_1} W + 2(1 - \rho)^2 W^T \Sigma_{a_2} W + 2\rho(1 - \rho) W^T (\Sigma_{a_1} + \Sigma_{a_2}) W]) \\
&= 4\nu_z \left[\nu_0 \sum_{i=1}^{d_0} w_i^4 + \alpha_1 \sum_{i=d_0+1}^{d_0+d_1} w_i^4 + \alpha_2 \sum_{i=d_0+d_1+1}^d w_i^4 \right];
\end{aligned} \tag{26}$$

$$\begin{aligned}
\mathbb{E}_{y_{ij}=0} [\operatorname{tr}(\Sigma_\mu)] &= \rho^2 \operatorname{tr}(2W^T \Sigma_{a_1} W) + (1 - \rho)^2 \operatorname{tr}(2W^T \Sigma_{a_2} W) + 2\rho(1 - \rho) \operatorname{tr}(W^T (\Sigma_{a_1} + \Sigma_{a_2}) W) \\
&= 2 \left[\nu_0 \sum_{i=1}^{d_0} w_i^2 + \alpha_1 \sum_{i=d_0+1}^{d_0+d_1} w_i^2 + \alpha_2 \sum_{i=d_0+d_1+1}^d w_i^2 \right],
\end{aligned} \tag{27}$$

and so

$$\begin{aligned}
\operatorname{tr}(\Sigma) \mathbb{E}_{y_{ij}=0} [\operatorname{tr}(\Sigma_\mu)] &= 4\nu_z \left(\sum_{i=1}^d w_i^2 \right) \left[\nu_0 \sum_{i=1}^{d_0} w_i^2 + \alpha_1 \sum_{i=d_0+1}^{d_0+d_1} w_i^2 + \alpha_2 \sum_{i=d_0+d_1+1}^d w_i^2 \right]; \tag{28} \\
\mathbb{E}_{y_{ij}=0} [\operatorname{tr}(\Sigma_\mu^2)] &= \rho^2 \operatorname{tr}((2W^T \Sigma_{a_1} W)^2) + (1 - \rho)^2 \operatorname{tr}((2W^T \Sigma_{a_2} W)^2) + 2\rho(1 - \rho) \operatorname{tr}((W^T (\Sigma_{a_1} + \Sigma_{a_2}) W)^2) \\
&= 2 \left[2\nu_0^2 \sum_{i=1}^{d_0} w_i^4 + \beta_1 \sum_{i=d_0+1}^{d_0+d_1} w_i^4 + \beta_2 \sum_{i=d_0+d_1+1}^d w_i^4 \right];
\end{aligned} \tag{29}$$

and similarly

$$\begin{aligned}
\mathbb{E}_{y_{ij}=0} [\operatorname{tr}^2(\Sigma_\mu)] &= 2 \left[2\nu_0^2 \left(\sum_{i=1}^{d_0} w_i^2 \right)^2 + \beta_1 \left(\sum_{i=d_0+1}^{d_0+d_1} w_i^2 \right)^2 + \beta_2 \left(\sum_{i=d_0+d_1+1}^d w_i^2 \right)^2 \right. \\
&\quad \left. + 4\gamma_{0,1} \sum_{i=1}^{d_0} w_i^2 \sum_{i=d_0+1}^{d_0+d_1} w_i^2 + 4\gamma_{0,2} \sum_{i=1}^{d_0} w_i^2 \sum_{i=d_0+d_1+1}^d w_i^2 + 4\gamma_{1,2} \sum_{i=d_0+1}^{d_0+d_1} w_i^2 \sum_{i=d_0+d_1+1}^d w_i^2 \right],
\end{aligned} \tag{30}$$

where we denote for short

$$\begin{aligned}
\gamma_{0,1} &:= \rho^2 \nu_0 \nu_1 + (1 - \rho)^2 \nu_0 \nu_2 + \rho(1 - \rho) \nu_0 (\nu_1 + \nu_2), \\
\gamma_{0,2} &:= \rho^2 \nu_0 \nu_2 + (1 - \rho)^2 \nu_0 \nu_1 + \rho(1 - \rho) \nu_0 (\nu_1 + \nu_2), \\
\gamma_{1,2} &:= \rho^2 \nu_1 \nu_2 + (1 - \rho)^2 \nu_1 \nu_2 + \frac{1}{2} \rho(1 - \rho) (\nu_1 + \nu_2)^2.
\end{aligned} \tag{31}$$

Finally, to symmetry, at the optimal solution we have

$$w_i = \begin{cases} u_0 & 0 \leq i \leq d_0 \\ u_1 & d_0 + 1 \leq i \leq d_0 + d_1 \\ u_2 & d_0 + d_1 + 1 \leq i \leq d \end{cases} \tag{32}$$

and by combining these results, we get

$$\begin{aligned}
\mathbb{E} \left[\tilde{\ell}(z_i, z_j, y_{ij}; d_g) \right] = & d_0 u_0^4 (8\nu_z^2 + 8\nu_z \nu_0 + 4\nu_0^2 + 2\nu_0^2 d_0) \\
& + d_1 u_1^4 (8\nu_z^2 + 8\nu_z \alpha_1 + 2\beta_1 + \beta_1 d_1) \\
& + d_2 u_2^4 (8\nu_z^2 + 8\nu_z \alpha_2 + 2\beta_2 + \beta_2 d_2) \\
& - 2d_0 u_0^2 (\nu_0 + \nu_z) - 2d_1 u_1^2 (\alpha_1 + \nu_z) - 2d_2 u_2^2 (\alpha_2 + \nu_z) \\
& + 4\nu_z^2 (d_0 u_0^2 + d_1 u_1^2 + d_2 u_2^2)^2 + \frac{1}{2} m \\
& + 4\nu_z (d_0 u_0^2 + d_1 u_1^2 + d_2 u_2^2) [\nu_0 d_0 u_0^2 + \alpha_1 d_1 u_1^2 + \alpha_2 d_2 u_2^2] \\
& + 4\gamma_{0,1} d_0 d_1 u_0^2 u_1^2 + 4\gamma_{0,2} d_0 d_2 u_0^2 u_2^2 + 4\gamma_{1,2} d_1 d_2 u_1^2 u_2^2.
\end{aligned} \tag{33}$$

B.2 Analysis of the Optimal Solution (Proof of Proposition 1)

Proposition 1 shows that for not too large values of d_2 , the optimal solution on the training distribution, assigns higher weight to components corresponding to high variance for training data, than to components corresponding to high variance on the shifted test distribution.

We begin by defining the required condition on d_2 . Denote

$$\begin{aligned}
\psi_1 &:= 2\nu_z^2 + 2\nu_z \alpha_1 + \beta_1 \\
\psi_2 &:= 2\nu_z^2 + 2\nu_z \alpha_2 + \beta_2 \\
\eta_{01} &:= 4\nu_z^2 + 2\nu_z (\alpha_1 + \nu_0) + 2\gamma_{0,1} \\
\eta_{02} &:= 4\nu_z^2 + 2\nu_z (\alpha_2 + \nu_0) + 2\gamma_{0,2} \\
\eta_{12} &:= 4\nu_z^2 + 2\nu_z (\alpha_1 + \alpha_2) + 2\gamma_{1,2}.
\end{aligned} \tag{34}$$

Then for α, β, γ values as in equations 24 and 31, we define

$$h(\rho, \nu_z, \nu_0, \nu_1, \nu_2, d_1) := \max \left\{ (2 + d_1) \frac{\psi_1 \eta_{02}}{\psi_2 \eta_{01}} - 2, (2 + d_1) \frac{\psi_1 \alpha_2 + \nu_z}{\psi_2 \alpha_1 + \nu_z} - 2, \frac{\eta_{12}}{2\psi_2} \right\}. \tag{35}$$

The condition on d_2 in Proposition 1 is that $d_2 \leq h(\rho, \nu_z, \nu_0, \nu_1, \nu_2, d_1)$. This provides a sufficient but not necessary condition – this is a simple example that does not require a full characterization of the optimal solution, which is provided in Appendix B.3.

Proof. Without loss of generality assume $m=1$. Then,

$$\begin{aligned}
\frac{\partial \mathbb{E} \left[\tilde{\ell}(z_i, z_j, y_{ij}; d_g) \right]}{\partial u_0^2} = & 2d_0 u_0^2 (8\nu_z^2 + 8\nu_z \nu_0 + 4\nu_0^2 + 2\nu_0^2 d_0) \\
& - 2d_0 (\nu_0 + \nu_z) \\
& + 8d_0 \nu_z^2 (d_0 u_0^2 + d_1 u_1^2 + d_2 u_2^2) \\
& + 4d_0 \nu_z (\nu_0 d_0 u_0^2 + \alpha_1 d_1 u_1^2 + \alpha_2 d_2 u_2^2) \\
& + 4d_0 \nu_z \nu_0 (d_0 u_0^2 + d_1 u_1^2 + d_2 u_2^2) \\
& + 4\gamma_{0,1} d_0 d_1 u_1^2 + 4\gamma_{0,2} d_0 d_2 u_2^2
\end{aligned} \tag{36}$$

and by setting the partial derivative to zero we get

$$\begin{aligned}
2u_0^2 (2 + d_0) (2\nu_z^2 + 2\nu_z \nu_0 + \nu_0^2) = & 2d_1 u_1^2 (2\nu_z^2 + \nu_z (\alpha_1 + \nu_0) + \gamma_{0,1}) \\
& + 2d_2 u_2^2 (2\nu_z^2 + \nu_z (\alpha_2 + \nu_0) + \gamma_{0,2}) - (\nu_0 + \nu_z).
\end{aligned} \tag{37}$$

Therefore,

$$u_0^2 = \frac{\nu_0 + \nu_z - \eta_{01} d_1 u_1^2 - \eta_{02} d_2 u_2^2}{2(2 + d_0)(2\nu_z^2 + 2\nu_z \nu_0 + \nu_0^2)}. \tag{38}$$

and similarly

$$u_1^2 = \frac{(\alpha_1 + \nu_z) - \eta_{01}d_0u_0^2 - \eta_{12}d_2u_2^2}{2(2+d_1)(2\nu_z^2 + 2\nu_z\alpha_1 + \beta_1)} \quad (39)$$

$$u_2^2 = \frac{(\alpha_2 + \nu_z) - \eta_{02}d_0u_0^2 - \eta_{12}d_1u_1^2}{2(2+d_2)(2\nu_z^2 + 2\nu_z\alpha_2 + \beta_2)}. \quad (40)$$

Hence,

$$\begin{aligned} d_1u_1^2 - d_2u_2^2 &= \frac{(2+d_2)(2\nu_z^2 + 2\nu_z\alpha_2 + \beta_2) [d_1(\alpha_1 + \nu_z) - \eta_{01}d_1d_0u_0^2 - \eta_{12}d_1d_2u_2^2]}{2(2+d_1)(2+d_2)(2\nu_z^2 + 2\nu_z\alpha_1 + \beta_1)(2\nu_z^2 + 2\nu_z\alpha_2 + \beta_2)} \\ &\quad - \frac{(2+d_1)(2\nu_z^2 + 2\nu_z\alpha_1 + \beta_1) [d_2(\alpha_2 + \nu_z) - \eta_{02}d_2d_0u_0^2 - \eta_{12}d_1d_2u_1^2]}{2(2+d_1)(2+d_2)(2\nu_z^2 + 2\nu_z\alpha_1 + \beta_1)(2\nu_z^2 + 2\nu_z\alpha_2 + \beta_2)}. \end{aligned} \quad (41)$$

Denoting

$$\begin{aligned} \xi &:= 2(2+d_1)(2+d_2)(2\nu_z^2 + 2\nu_z\alpha_1 + \beta_1)(2\nu_z^2 + 2\nu_z\alpha_2 + \beta_2) \\ &= 2(2+d_1)(2+d_2)\psi_1\psi_2 \end{aligned}$$

we have

$$\begin{aligned} d_1u_1^2 \left[1 - \frac{1}{\xi}(2+d_1)\psi_1\eta_{12} \right] &= d_2u_2^2 \left[1 - \frac{1}{\xi}(2+d_2)\psi_2\eta_{12} \right] \\ &\quad + \frac{1}{\xi}(2+d_2)\psi_2(\alpha_1 + \nu_z) - \frac{1}{\xi}(2+d_1)\psi_1(\alpha_2 + \nu_z) \\ &\quad + d_0u_0^2 \left[\frac{1}{\xi}(2+d_1)\psi_1\eta_{02} - \frac{1}{\xi}(2+d_2)\psi_2\eta_{01} \right] \end{aligned}$$

and therefore

$$\begin{aligned} d_1u_1^2 - d_2u_2^2 &= d_2u_2^2 \left(\frac{1 - \frac{1}{\xi}(2+d_2)\psi_2\eta_{12}}{1 - \frac{1}{\xi}(2+d_1)\psi_1\eta_{12}} - 1 \right) \\ &\quad + \frac{1}{2(2+d_1)(2+d_2)\psi_1\psi_2} \frac{(2+d_2)\psi_2(\alpha_1 + \nu_z) - (2+d_1)\psi_1(\alpha_2 + \nu_z)}{1 - \frac{1}{\xi}(2+d_1)\psi_1\eta_{12}} \\ &\quad + d_0u_0^2 \frac{1}{2(2+d_1)(2+d_2)\psi_1\psi_2} \left[\frac{(2+d_1)\psi_1\eta_{02}}{1 - \frac{1}{\xi}(2+d_1)\psi_1\eta_{12}} - \frac{(2+d_2)\psi_2\eta_{01}}{1 - \frac{1}{\xi}(2+d_1)\psi_1\eta_{12}} \right]. \end{aligned} \quad (42)$$

Since $\eta_{02} \leq \eta_{01}$ the assumption $(2+d_2)\psi_2\eta_{01} \leq (2+d_1)\psi_1\eta_{02}$ also yields $(2+d_2)\psi_2 \leq (2+d_1)\psi_1$. Hence, for

$$d_2 + 2 < \max \left\{ (2+d_1)\frac{\psi_1}{\psi_2}\frac{\eta_{02}}{\eta_{01}}, (2+d_1)\frac{\psi_1}{\psi_2}\frac{\alpha_2 + \nu_z}{\alpha_1 + \nu_z}, \frac{\eta_{12}}{2\psi_2} \right\}$$

all the terms in 42 are positive and therefore $d_1u_1^2 - d_2u_2^2 > 0$. \square

B.3 Explicit Expression for the Optimal Representation

In order to derive the optimal representation, we differentiate the expected loss with respect to the squared values in the diagonal of W , that is, w_i^2 :

$$\frac{\partial}{\partial (w_i^2)} \text{tr}(\Sigma^2) = 8\nu_z^2 w_i^2 \quad (43)$$

$$\frac{\partial}{\partial (w_i^2)} \text{tr}^2(\Sigma) = 8\nu_z^2 \sum_{j=1}^d w_j^2 \quad (44)$$

$$\frac{\partial}{\partial (w_i^2)} \mathbb{E}_{y=0} [\text{tr}(\Sigma \Sigma_\mu)] = \begin{cases} 8\nu_z \nu_0 w_i^2 & 1 \leq i \leq d_0 \\ 8\nu_z \alpha_1 w_i^2 & d_0 + 1 \leq i \leq d_0 + d_1 \\ 8\nu_z \alpha_2 w_i^2 & d_0 + d_1 + 1 \leq i \leq d \end{cases} \quad (45)$$

$$\frac{\partial [\text{tr}(\Sigma) \mathbb{E}_{y=0} [\text{tr} \Sigma_\mu]]}{\partial (w_i^2)} = \begin{cases} 4\nu_z \left[2\nu_0 \sum_{j=1}^{d_0} w_j^2 + (\alpha_1 + \nu_0) \sum_{j=d_0+1}^{d_0+d_1} w_j^2 + (\alpha_2 + \nu_0) \sum_{j=d_0+d_1+1}^d w_j^2 \right] & 1 \leq i \leq d_0 \\ 4\nu_z \left[(\nu_0 + \alpha_1) \sum_{j=1}^{d_0} w_j^2 + 2\alpha_1 \sum_{j=d_0+1}^{d_0+d_1} w_j^2 + (\alpha_2 + \alpha_1) \sum_{j=d_0+d_1+1}^d w_j^2 \right] & d_0 + 1 \leq i \leq d_0 + d_1 \\ 4\nu_z \left[(\nu_0 + \alpha_2) \sum_{j=1}^{d_0} w_j^2 + (\alpha_1 + \alpha_2) \sum_{j=d_0+1}^{d_0+d_1} w_j^2 + 2\alpha_2 \sum_{j=d_0+d_1+1}^d w_j^2 \right] & d_0 + d_1 + 1 \leq i \leq d \end{cases} \quad (46)$$

$$\frac{\partial}{\partial (w_i^2)} \mathbb{E}_{y=0} [\text{tr}(\Sigma_\mu^2)] = \begin{cases} 8\nu_0^2 w_i^2 & 1 \leq i \leq d_0 \\ 4\beta_1 w_i^2 & d_0 + 1 \leq i \leq d_0 + d_1 \\ 4\beta_2 w_i^2 & d_0 + d_1 + 1 \leq i \leq d \end{cases} \quad (47)$$

$$\frac{\partial}{\partial (w_i^2)} \mathbb{E}_{y=0} [\text{tr}^2(\Sigma_\mu)] = \begin{cases} 8\nu_0^2 \sum_{j=1}^{d_0} w_j^2 + 8\gamma_{0,1} \sum_{j=d_0+1}^{d_0+d_1} w_j^2 + 8\gamma_{0,2} \sum_{j=d_0+d_1+1}^d w_j^2 & 1 \leq i \leq d_0 \\ 8\gamma_{0,1} \sum_{j=1}^{d_0} w_j^2 + 4\beta_1 \sum_{j=d_0+1}^{d_0+d_1} w_j^2 + 8\gamma_{1,2} \sum_{j=d_0+d_1+1}^d w_j^2 & d_0 + 1 \leq i \leq d_0 + d_1 \\ 8\gamma_{0,2} \sum_{j=1}^{d_0} w_j^2 + 8\gamma_{1,2} \sum_{j=d_0+1}^{d_0+d_1} w_j^2 + 4\beta_2 \sum_{j=d_0+d_1+1}^d w_j^2 & d_0 + d_1 + 1 \leq i \leq d \end{cases} \quad (48)$$

Combining these results, we get for $1 \leq i \leq d_0$

$$\begin{aligned} \partial_0 &:= \frac{\partial}{\partial (w_i^2)} \tilde{\ell}(z_i, z_j, y_{ij}; d_g) = \frac{1}{2} \left[2 \cdot 8\nu_z^2 w_i^2 + 8\nu_z^2 \sum_{j=1}^d w_j^2 \right] - m [2(\nu_0 + \nu_z)] \\ &\quad + 8\nu_z^2 w_i^2 + 4\nu_z^2 \sum_{j=1}^d w_j^2 + 2 \cdot 8\nu_z \nu_0 w_i^2 \\ &\quad + 4\nu_z \left[2\nu_0 \sum_{j=1}^{d_0} w_j^2 + (\alpha_1 + \nu_0) \sum_{j=d_0+1}^{d_0+d_1} w_j^2 + (\alpha_2 + \nu_0) \sum_{j=d_0+d_1+1}^d w_j^2 \right] \\ &\quad + 8\nu_0^2 w_i^2 + \frac{1}{2} \left[8\nu_0^2 \sum_{j=1}^{d_0} w_j^2 + 8\gamma_{0,1} \sum_{j=d_0+1}^{d_0+d_1} w_j^2 + 8\gamma_{0,2} \sum_{j=d_0+d_1+1}^d w_j^2 \right], \end{aligned}$$

for $d_0 + 1 \leq i \leq d_0 + d_1$

$$\begin{aligned}\partial_1 := \frac{\partial}{\partial(w_i^2)} \tilde{\ell}(z_i, z_j, y_{ij}; d_g) &= \frac{1}{2} \left[2 \cdot 8\nu_z^2 w_i^2 + 8\nu_z^2 \sum_{j=1}^d w_j^2 \right] - m[2(\alpha_1 + \nu_z)] \\ &\quad + 8\nu_z^2 w_i^2 + 4\nu_z^2 \sum_{j=1}^d w_j^2 + 2 \cdot 8\nu_z \alpha_1 w_i^2 \\ &\quad + 4\nu_z \left[(\nu_0 + \alpha_1) \sum_{j=1}^{d_0} w_j^2 + 2\alpha_1 \sum_{j=d_0+1}^{d_0+d_1} w_j^2 + (\alpha_2 + \alpha_1) \sum_{j=d_0+d_1+1}^d w_j^2 \right] \\ &\quad + 4\beta_1 w_i^2 + \frac{1}{2} \left[8\gamma_{0,1} \sum_{j=1}^{d_0} w_j^2 + 4\beta_1 \sum_{j=d_0+1}^{d_0+d_1} w_j^2 + 8\gamma_{1,2} \sum_{j=d_0+d_1+1}^d w_j^2 \right],\end{aligned}$$

and similarly for $d_0 + d_1 + 1 \leq i \leq d$

$$\begin{aligned}\partial_2 := \frac{\partial}{\partial(w_i^2)} \tilde{\ell}(z_i, z_j, y_{ij}; d_g) &= \frac{1}{2} \left[2 \cdot 8\nu_z^2 w_i^2 + 8\nu_z^2 \sum_{j=1}^d w_j^2 \right] - m[2(\alpha_2 + \nu_z)] \\ &\quad + 8\nu_z^2 w_i^2 + 4\nu_z^2 \sum_{j=1}^d w_j^2 + 2 \cdot 8\nu_z \alpha_2 w_i^2 \\ &\quad + 4\nu_z \left[(\nu_0 + \alpha_2) \sum_{j=1}^{d_0} w_j^2 + (\alpha_1 + \alpha_2) \sum_{j=d_0+1}^{d_0+d_1} w_j^2 + 2\alpha_2 \sum_{j=d_0+d_1+1}^d w_j^2 \right] \\ &\quad + 4\beta_2 w_i^2 + \frac{1}{2} \left[8\gamma_{0,2} \sum_{j=1}^{d_0} w_j^2 + 8\gamma_{1,2} \sum_{j=d_0+1}^{d_0+d_1} w_j^2 + 4\beta_2 \sum_{j=d_0+d_1+1}^d w_j^2 \right].\end{aligned}$$

and thus we can write for the symmetric solution

$$\partial_0 = -2m(\nu_0 + \nu_z) + u_0^2 A_{0,0} + u_1^2 A_{0,1} + u_2^2 A_{0,2}, \quad (49)$$

$$\partial_1 = -2m(\alpha_1 + \nu_z) + u_0^2 A_{1,0} + u_1^2 A_{1,1} + u_2^2 A_{1,2}, \quad (50)$$

$$\partial_2 = -2m(\alpha_2 + \nu_z) + u_0^2 A_{2,0} + u_1^2 A_{2,1} + u_2^2 A_{2,2}, \quad (51)$$

where

$$A_{0,0} = 16\nu_z^2 + 8\nu_z^2 d_0 + 16\nu_z \nu_0 + 8\nu_z \nu_0 d_0 + 8\nu_0^2 + 4\nu_0^2 d_0$$

$$A_{0,1} = 8\nu_z^2 d_1 + 4\nu_z(\alpha_1 + \nu_0) d_1 + 4\gamma_{0,1} d_1$$

$$A_{0,2} = 8\nu_z^2 d_2 + 4\nu_z(\alpha_2 + \nu_0) d_2 + 4\gamma_{0,2} d_2$$

$$A_{1,0} = 8\nu_z^2 d_0 + 4\nu_z(\nu_0 + \alpha_1) d_0 + 4\gamma_{0,1} d_0$$

$$A_{1,1} = 16\nu_z^2 + 8\nu_z^2 d_1 + 16\nu_z \alpha_1 + 8\nu_z \alpha_1 d_1 + 4\beta_1 + 4\beta_1 d_1$$

$$A_{1,2} = 8\nu_z^2 d_2 + 4\nu_z(\alpha_2 + \alpha_1) d_2 + 4\gamma_{1,2} d_2$$

$$A_{2,0} = 8\nu_z^2 d_0 + 4\nu_z(\nu_0 + \alpha_2) d_0 + 4\gamma_{0,2} d_0$$

$$A_{2,1} = 8\nu_z^2 d_1 + 4\nu_z(\alpha_1 + \alpha_2) d_1 + 4\gamma_{1,2} d_1$$

$$A_{2,2} = 16\nu_z^2 + 8\nu_z^2 d_2 + 16\nu_z \alpha_2 + 8\nu_z \alpha_2 d_2 + 4\beta_2 + 4\beta_2 d_2.$$

Therefore, the optimal representation is given by the solution to the following set of linear equations:

$$\begin{pmatrix} u_0^2 \\ u_1^2 \\ u_2^2 \end{pmatrix} = 2m A^{-1} \begin{pmatrix} \nu_0 + \nu_z \\ \alpha_1 + \nu_z \\ \alpha_2 + \nu_z \end{pmatrix}, \quad (52)$$

Table 1: Simulation results. For each mixture ratio we report the mean AUC and (in brackets) the standard deviation across 10 repetitions of the experiment. Results are reported for in-distribution scenario (P_C), and class distribution shift (Q_C). Best result is marked in bold.

		$\rho = 0.05$	$\rho = 0.1$	$\rho = 0.3$
In Distribution	ERM	0.948±0.013	0.948±0.007	0.913±0.017
	Hier	0.945±0.013	0.949 ±0.010	0.917 ±0.016
	IRM	0.945±0.013	0.947±0.009	0.909±0.018
	CLOvE	0.944±0.008	0.949±0.011	0.911±0.020
	VarREx	0.949±0.013	0.948±0.009	0.910±0.022
	VarAUC	0.950 ±0.017	0.947±0.008	0.912±0.022
Distribution Shift	ERM	0.731±0.007	0.808±0.015	0.883±0.014
	Hier	0.727±0.009	0.810±0.014	0.882±0.020
	IRM	0.724±0.017	0.806±0.019	0.880±0.023
	CLOvE	0.745±0.020	0.807±0.018	0.878±0.020
	VarREx	0.729±0.005	0.811±0.018	0.880±0.026
	VarAUC	0.767 ±0.008	0.838 ±0.019	0.881 ±0.024

where

$$A = \begin{pmatrix} A_{0,0} & A_{0,1} & A_{0,2} \\ A_{1,0} & A_{1,1} & A_{1,2} \\ A_{2,0} & A_{2,1} & A_{2,2} \end{pmatrix}. \quad (53)$$

C Comparison to OOD Environment Balancing Methods

Previous methods in the field of OOD generalization (see §2) exhibit several key differences compared to our setting: (i) They address closed-world classification, whereas in zero-shot learning, new classes are encountered. (ii) The presumed shift is typically in the conditional distribution of the data given the class (e.g., the background given the class being a cow or a camel), whereas we consider shifts in the class distribution $P(c)$. (iii) Existing methods often assume that training data comes from various data environments, providing explicit information about how the distribution might shift, while we assume the attribute A causing the shift is unknown.

Despite these differences, in this work we recast class distribution shifts in zero-shot learning into environment balancing OOD setting, by making the following observations. First, when posed as verification methods, zero-shot classifiers in fact perform a binary (closed-world) classification task, predicting whether a pair of data points $x_{ij} := (z_i, z_j)$ belong to the same class $y_{ij} = \mathbb{1}_{c_i=c_j}$.

Note that the distribution of possible pairs $x_{ij} = (z_i, z_j)$ given the label y_{ij} changes with variations in class attribute probabilities, and therefore across synthetic environments S . Thus, in this formulation the shift occurs in the conditional distribution of the data given the class $p(x_{ij}|y_{ij})$.

Another distinction lies in data availability: in the setting of closed-world OOD environment balancing methods, a main drawback is the challenge of securing a sufficient number of diverse training environments. This is essential to ensure that a representation performing well on observed environments, will likely perform similarly on unobserved ones. In contrast, our framework allows for the construction of many synthetic environments via sampling.

D Additional Empirical Results

D.1 Additional Simulation Results

Simulations Exact mean and standard deviations matching Figure 4 are provided in table 1.

AUC progress during training iterations and feature importance results for the majority class proportion of $\rho = 0.1$ were shown in the main text. Here, we provide analogous results for $\rho = 0.05$ and $\rho = 0.3$. These are summarized in Figure 8.

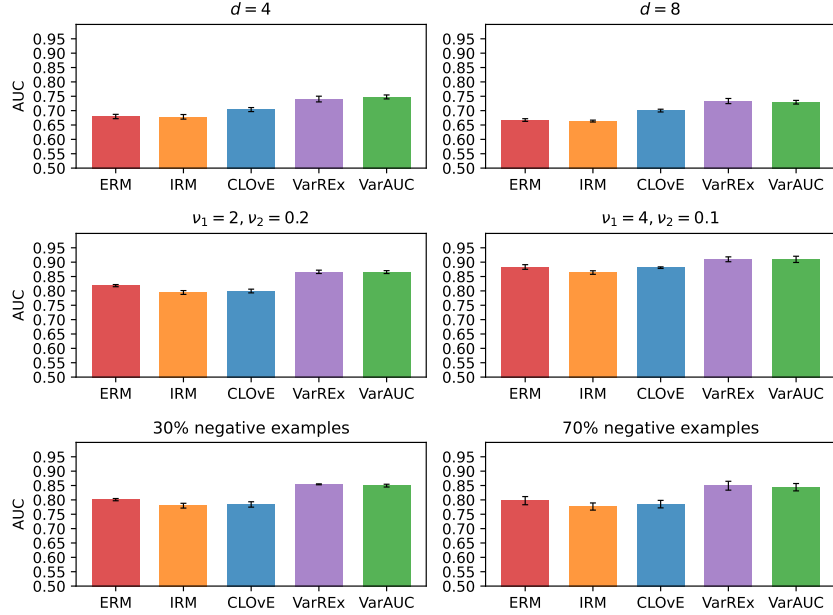


Figure 7: Additional simulation results. Top row: Additional dimensions of the representation. Middle row: additional ratios of the attribute variances. Bottom row: unbalanced sets of positive and negative examples. Bars show mean AUC values on the test set across 5 repetitions of the experiment, whiskers show \pm standard deviation.

For $\rho = 0.05$ the convergence results are similar to those obtained for $\rho = 0.1$ – under distribution-shift the two variance based methods show significantly better results compared to other approaches. Our algorithm with the VarREx penalty achieves high AUC values more quickly than the VarAUC penalty, but the VarAUC penalty attains higher accuracy overall. The CLOvE penalty achieves improvement over ERM, but smaller compared to the variance based methods. IRM converges to the same AUC as ERM. In contrast, on in-distribution data all methods perform well.

For $\rho = 0.3$ the distribution shift is milder and therefore ERM performs very well (0.902 AUC is achieved on distribution shift scenario compared to 0.932 on in-distribution setting). Therefore encouragement of similar performance across different data subsets does not benefit the learning process. Slightly better result is achieved with VarREx penalty (0.911).

The analysis of feature importance for $\rho = 0.05$ yields results similar to those for $\rho = 0.1$. At $\rho = 0.3$ the analysis remains mostly unchanged, except that VarREx assigns higher importance to features corresponding to ν_0 (0-5) compared to VarAUC, while in more extreme distribution shifts VarAUC assigns higher importance to the shared features.

D.2 Additional Representation Sizes, Noise Ratios and Positive Proportions

In §5.1 we explored varying values of ρ in a setting where $\nu^+ = 2$, $\nu^- = 0.1$ ($\frac{\nu^+}{\nu^-} = 20$). We now focus on the case of $\rho = 0.1$ and examine additional representation sizes p , and noise ratios ($\frac{\nu^+}{\nu^-} \in \{10, 40\}$). Additionally, we examine the original setting where $p = 16$ and $\nu^+ = 2$, $\nu^- = 0.1$, with varying proportions of positive and negative examples.

The results in Figure 7 show that in all the additional settings our methods provides statistically significant improvement over the baseline. FDR adjusted p-values for multiple comparisons are provided in Table 2.

Table 2: FDR adjusted p-values for the results reported in Figure 7

Experiment	IRM	CLOvE	VarREx	VarAUC
$p = 4$	0.7339	0.0112	0.0003	0.0001
$p = 8$	0.8552	0.0005	0.0003	0.0001
$\nu_1 = 2, \nu_2 = 0.2$	0.9995	0.9995	0.0002	<0.0001
$\nu_1 = 4, \nu_2 = 0.1$	0.9989	0.9971	0.0041	0.0041
30% negative	0.9939	0.9939	<0.0001	<0.0001
70% negative	1.0	1.0	<0.0001	0.0002

Experiments In Table 3, we provide the means and standard deviations for the experiments detailed in §5.2. Additionally, Table 4 presents the adjusted p-values for assessing the performance increase over the ERM baseline achieved by our algorithm with the explored penalties.

Table 3: Experimental results. Mean and (in brackets) standard deviation of AUC values over 5 repetitions are reported for in distribution scenario (P_C), and class distribution shift (Q_C). Best result is marked in bold.

		IN DISTRIBUTION	DISTRIBUTION SHIFT
CELEBA	ERM	0.826 ± 0.001	0.666 ± 0.001
	IRM	0.843 ± 0.009	0.659 ± 0.087
	CLOvE	0.853 ± 0.002	0.677 ± 0.012
	VARREx	0.834 ± 0.002	0.676 ± 0.004
	VARAUC	0.836 ± 0.002	0.697 ± 0.027
ETHEC	ERM	0.869 ± 0.004	0.786 ± 0.030
	IRM	0.879 ± 0.004	0.795 ± 0.034
	CLOvE	0.888 ± 0.004	0.800 ± 0.040
	VARREx	0.877 ± 0.007	0.805 ± 0.033
	VARAUC	0.872 ± 0.004	0.838 ± 0.049

Table 4: Adjusted p-values for one-sided paired t-tests for testing the improvements over the ERM baseline.

	CELEBA	ETHEC
HIERARCHICAL	0.0154	0.7677
IRM	0.6117	0.1290
CLOvE	0.0119	0.0383
VARREx	< 0.0001	0.0383
VARAUC	0.0058	0.0383

D.3 Analysis of Loss Values

Here we present an analysis of the unpenalized loss after convergence in both real-data experiments. We performed separate analyses on pairs of data points from the dominant type during training (majority), and those from the other type (minority). Additionally, we separated positive pairs ($y = 1$) and negative pairs ($y = 0$). Figure 9 displays histograms illustrating the differences between losses on the training set obtained with the representation learned using ERM (g_{ERM}), and those obtained using our algorithm with VarAUC penalty (g_{VarAUC}):

$$\text{Diff}_{ij} = \ell(x_{ij}, y_{ij}; d_{g_{\text{ERM}}}) - \ell(x_{ij}, y_{ij}; d_{g_{\text{VarAUC}}}).$$

Positive values of the differences correspond to higher losses for ERM.

In both experiments, when examining negative pairs from the minority group, as shown in the top-left histograms, most of the observed differences are positive. This indicates that the ERM losses for these pairs are higher compared to the losses obtained for the representation trained with the VarAUC

penalty. The disparities are smaller for the other three groups: majority negative pairs, minority negative pairs, and minority positive pairs. Among these groups, ERM performs better on positive pairs.

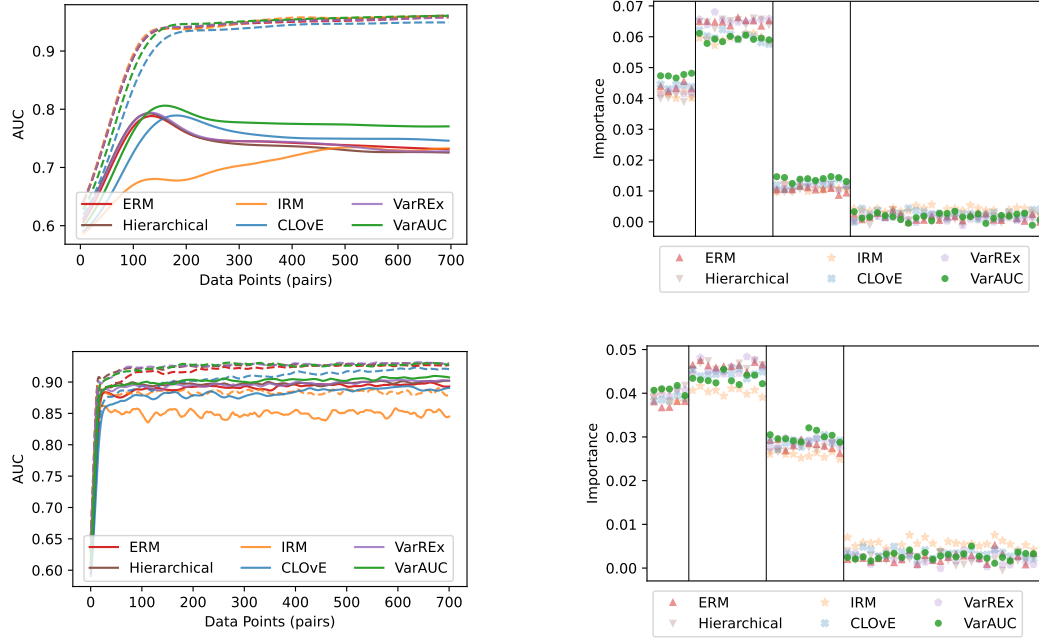


Figure 8: Additional Simulation Results. Top row: $\rho = 0.05$, Bottom row: $\rho = 0.3$. Left: Average AUC progress over 10 repetitions of the simulation. Solid lines correspond to performance on test data (distribution shift scenario), dashed lines show performance on data sampled from the same distribution as training data (in-distribution scenario). Right: Average feature importance results over 10 repetitions.

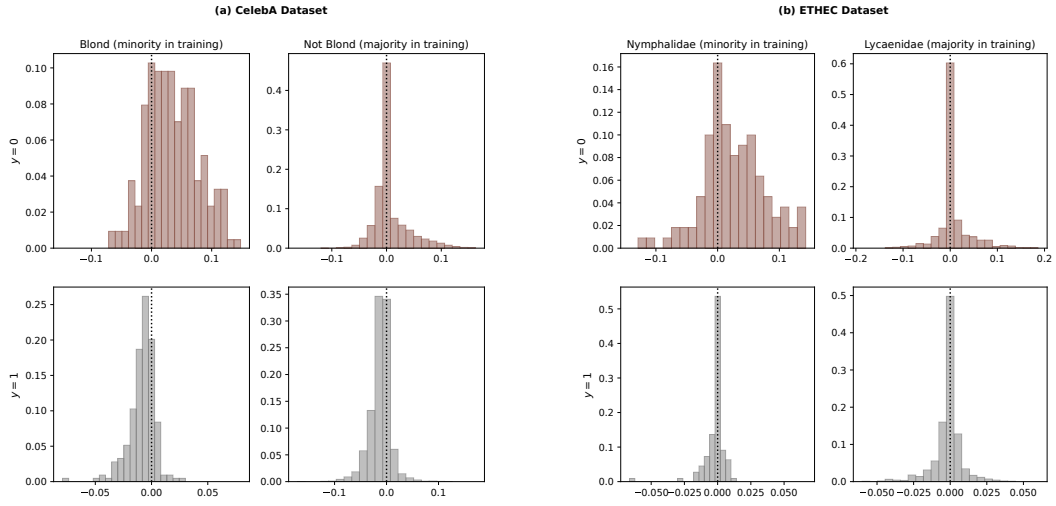


Figure 9: Analysis of Loss Differences. Histograms of differences between ERM and our algorithm with VarAUC penalty are shown for two experiments in separate sub-figures: (a) CelebA dataset, (b) ETHEC dataset. The top rows show differences for negative pairs ($y = 0$), bottom ones show differences for positive pairs ($y = 1$). In each sub-figure the left column corresponds to the minority type and right one to the majority. A dotted black line marks a difference of 0. Positive values correspond to higher losses for ERM.

E Datasets

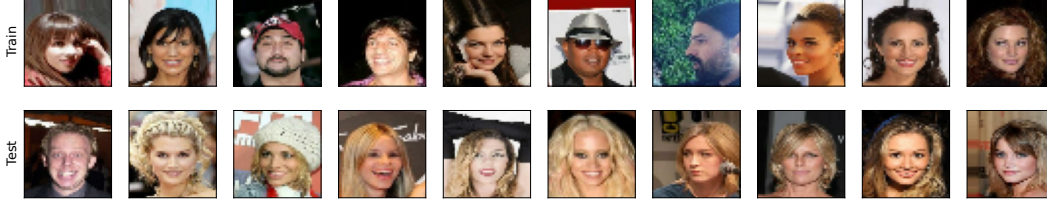


Figure 10: Sample Images from the CelebA Dataset. Top: a random sample of the training data with 95% non-blond people. Bottom: a random sample of the test data with 95% blond people.

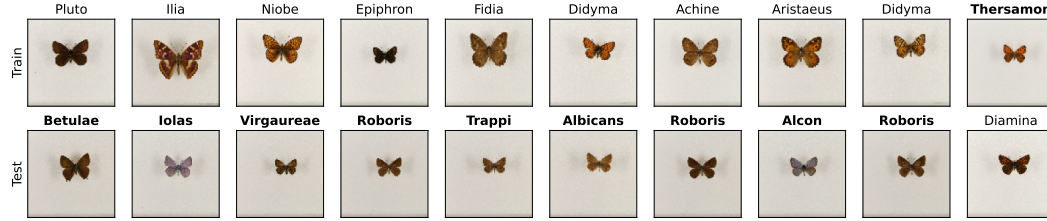


Figure 11: Sample Images from the ETHEC Dataset. Top: a sample of the the training data – 9 species of the Lycaenidae family and 1 from the Nymphalidae family. Bottom: a sample of the test data where the proportion of the families is reversed. Nymphalidae species names are marked in bold.

F Implementation Details

Code to reproduce our results is attached to the submission and upon acceptance a link to a permanent repository will be included in the main text.

The data-related parameters of our experiments are described in the main text. In all our experiments we used margin of $m = 0.5$ for the contrastive loss and Adam (Kingma & Ba, 2014) optimizer to train all models.

For the CLOvE penalty we used a Laplacian kernel $k(r, r') = e^{\frac{1}{\text{width}} - |r - r'|}$ with width of 0.4 as originally suggested by Kumar et al. (2018).

For optimization of the VarAUC objective we disregard the finite sample correction $\frac{N_s - n}{N_s - 1}$ in the implementation since n is very small compared to N_s . In practice, we minimize the standard deviation instead of the variance in both variance based penalties, and the hyperparameters are reported accordingly.

In our scenario where the attribute of interest is unknown, we generated a synthetic attribute for hyperparameter selection using Principle Components (PC). We ranked examples based on their first PC component values, classifying the top 10% as positive and the rest as negative. Hyperparameters for all methods were chosen via grid-search in a single experiment repetition, ensuring robustness against this synthetic attribute. Notably, the experiments themselves did not involve the PC attribute; instead, they focused on dimension swapping in simulations and attributes like hair color or species family in CelebA and ETHEC experiments.

The grid search produced almost identical hyperparameters for all three ρ values. We observed that performance converged to the same value when employing hyperparameters derived from cross-validation for one ρ value, as those selected for another. Therefore, for simplicity we repeated simulations using the same hyperparameters, determined based on the grid search results for $\rho = 0.1$ (the intermediate parameter value). Similarly, minimal differences in optimal learning rates were observed among the methods within an experiment and therefore a shared learning rate was used for each experiment. To emphasize the improvement of OOD methods over the ERM baseline, we

used the learning rate optimized for the ERM method. Large differences were observed in optimal regularization factors, and therefore these parameters (as well as method-specific parameters) were not shared. All hyper-parameters are reported in Table 5.

All models were initialized with identical weights, and trained on identical data splits.

All the code in this work was implemented in Python 3.10. We used the TensorFlow 2.13 and TensorFlow Addons 0.21 packages. For evaluation we used the auc function from scikit-learn 1.2. The CelebA dataset was loaded through TensorFlow Datasets 4.9 and pandas 1.5 was used to process the ETHEC dataset. Statistical tests were performed using ttest_rel and false_discovery_control functions from scipy.stats 1.11.4. All figures were generated using Matplotlib 3.7.

The IRM implementation was adapted from the source code of the paper, available at <https://github.com/facebookresearch/InvariantRiskMinimization>.

We ran all experiments on a single A100 cloud GPU. For simulations, each full repetition of the experiment (comparing all methods) required on average 2.06 hours. Each repetition on the ETHEC dataset took 7.38 hours on average, and on the CelebA dataset 11.52 hours.

Table 5: Hyper Parameters.

		ERM	IRM	CLOVE	VARREX	VARAUC
SIMULATIONS	LEARNING RATE η	0.01	0.01	0.01	0.01	0.01
	REGULARIZATION FACTOR λ	—	0.01	0.05	3.0	1.5
	NETWORK WEIGHT REGULARIZER	—	0.01	—	—	—
CELEBA	LEARNING RATE η	10^{-5}	10^{-5}	10^{-5}	10^{-5}	10^{-5}
	REGULARIZATION FACTOR λ	—	0.1	0.085	0.01	0.2
	NETWORK WEIGHT REGULARIZER	—	0.01	—	—	—
ETHEC	LEARNING RATE η	10^{-3}	10^{-3}	10^{-3}	10^{-3}	10^{-3}
	REGULARIZATION FACTOR λ	—	0.02	0.05	0.1	0.2
	NETWORK WEIGHT REGULARIZER	—	0.01	—	—	—